Article

Formation of Third Generation Poly(pyrazolyl)borate Ligands from Alkyne Coupling Reactions of Fe[(*p*-ICH)B(3-Rpz)] (R = H, Me; pz = Pyrazolyl): Pathways toward Controlling an Iron(II) Electronic Spin-State Crossover

Daniel L. Reger, James R Gardinier, William R. Gemmill, Mark D. Smith, Ahmed M. Shahin, Gary J. Long, Leila Rebbouh, and Fernande Grandjean

J. Am. Chem. Soc., **2005**, 127 (7), 2303-2316• DOI: 10.1021/ja044900h • Publication Date (Web): 29 January 2005

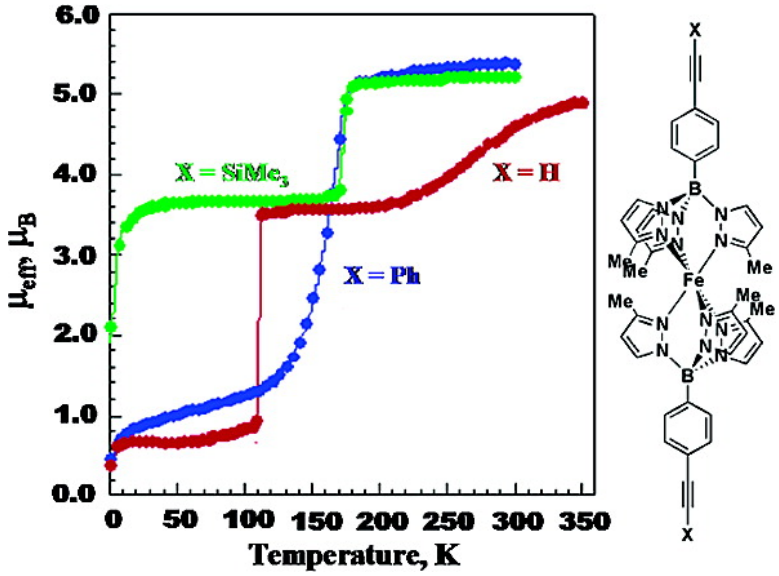

More About This Article

Additional resources and features associated with this article are available within the HTML version:

- Supporting Information
- Links to the 9 articles that cite this article, as of the time of this article download
- Access to high resolution figures
- Links to articles and content related to this article
- Copyright permission to reproduce figures and/or text from this article

View the Full Text HTML

J|A|C|S
ARTICLES
Published on Web 01/29/2005

Formation of Third Generation Poly(pyrazolyl)borate Ligands from Alkyne Coupling Reactions of Fe[(*p*-IC$_6$H$_4$)B(3-Rpz)$_3$]$_2$ (R = H, Me; pz = Pyrazolyl): Pathways toward Controlling an Iron(II) Electronic Spin-State Crossover

Daniel L. Reger,*[†] James R Gardinier,[†] William R. Gemmill,[†] Mark D. Smith,[†] Ahmed M. Shahin,[‡] Gary J. Long,*[‡] Leila Rebbouh,[§] and Fernande Grandjean[§]

Contribution from the Department of Chemistry and Biochemistry, University of South Carolina, Columbia, South Carolina 29208; Department of Chemistry, University of Missouri−Rolla, Rolla, Missouri 65409-0010; and Department of Physics, B5, University of Liège, B-4000 Sart-Tilman, Belgium

Received August 24, 2004; E-mail: reger@mail.chem.sc.edu; glong@umr.edu

Abstract: Sonogashira coupling reactions of terminal alkynes with Fe[(*p*-IC$_6$H$_4$)B(3-Mepz)$_3$]$_2$ (pz = pyrazolyl ring) yield Fe[(*p*-PhC$_2$C$_6$H$_4$)B(3-Mepz)$_3$]$_2$ (**2**), Fe[(*p*-Me$_3$SiC$_2$C$_6$H$_4$)B(3-Rpz)$_3$]$_2$ (R = H, **3a**, R = Me, **3b**), and Fe[(*p*-HC$_2$C$_6$H$_4$)B(3-Mepz)$_3$]$_2$ (R = H, **4a**, R = Me, **4b**), a series of new complexes containing "third generation" poly(pyrazolyl)borate ligands. Complex **2** undergoes a fairly gradual iron(II) electronic spin-state crossover with a 30 K hysteresis, whereas complex **3b** is an unusual example of a complex with equivalent iron(II) sites in the high-spin form that shows an abrupt 50% spin crossover. For complex **4b**, 50% of the iron(II) sites undergo a gradual spin-state transition between 185 and 350 K with an activation energy of 1590 ± 30 cm^{-1} and a $T_{1/2}$ = 280 K and, for the remaining iron(II) sites, an abrupt cooperative spin-state crossover between 106 and 114 K. The crystal structures of **4b** obtained for each of the three distinct electronic spin states reveal two crystallographically different iron(II) sites, and analysis of the molecular/supramolecular structures indicates that the difference in the degree of pyrazolyl ring tilting in the ligands between the two sites, rather than the strength of the intermolecular forces, play a prominent role in determining the temperature of the spin-state crossover.

Introduction

Iron(II) spin-state crossover complexes have garnered much research attention lately because of their potential technological applications.[1] The spin-state crossover in iron(II) complexes was first discovered in the 1960s, and since then, much research effort has involved trying to predict, model, and/or control the temperature dependence of the photochromic and/or thermochromic $t_{2g}^6e_g^{*0}$ to $t_{2g}^4e_g^{*2}$ electronic transition.[2] As part of our studies on the use of specifically designed tris(pyrazolyl)methane and tris(pyrazolyl)borate ligands to support unusual supramolecular structures,[3−5] we have recently shown[6] that the supramolecular organization of iron(II) complexes can have a profound impact on the electronic spin-state crossover properties of a tris(pyrazolyl)borate iron(II) complex, namely of polymorphs of Fe[(*p*-IC$_6$H$_4$)B(3-Mepz)$_3$]$_2$, **1b** (pz = pyrazolyl ring). Specifically, for these two polymorphs, the more highly organized structure did not undergo the spin-state crossover, whereas the more "loosely" organized structure did. The impact of supramolecular structure on spin-state crossover properties has been discussed in a few other systems.[7]

To further explore the effect of supramolecular organization on the spin-state crossover properties of iron(II) complexes of tris(pyrazolyl)borate ligands, we have explored the chemistry of the *p*-iodo group in Fe[(*p*-IC$_6$H$_4$)B(3-Mepz)$_3$]$_2$ with the goal of preparing substituted derivatives containing functional groups

[†] University of South Carolina.
[‡] University of Missouri−Rolla.
[§] University of Liège.

(1) (a) Muller, R. N.; Van der Elst, L.; Laurent, S. *J. Am. Chem. Soc.* **2003**, *125*, 8405. (b) Kahn, O.; Martinez, C. J. *Science* **1998**, *279*, 44.
(2) For leading reviews, see: (a) Real, J. A.; Gaspar, A. B.; Niel, V.; Muñoz, M. C. *Coord. Chem. Rev.* **2003**, *236*, 121. (b) Gütlich, P.; Garcia, Y.; Goodwin, H. A. *Chem. Soc. Rev.* **2000**, *29*, 419. (c) Gütlich, P.; Hauser, A.; Spiering, H. *Angew. Chem., Int. Ed. Engl.* **1994**, *33*, 2024. (d) König, E.; Ritter, G.; Kulshreshtha, S. K. *Chem. Rev.* **1985**, *85*, 219. (e) Long, G. J.; Grandjean, F.; Reger, D. L. *Top. Curr. Chem.* **2004**, *233*, 91.
(3) (a) Reger, D. L.; Semeniuc, R. F.; Rassolov, V.; Smith, M. D. *Inorg. Chem.* **2004**, *43*, 537. (b) Reger, D. L.; Semeniuc, R. F.; Smith, M. D. *Inorg. Chem.* **2003**, *42*, 8137. (c) Reger, D. L.; Semeniuc, R. F.; Silaghi-Dumitrescu, I.; Smith, M. D. *Inorg. Chem.* **2003**, *42*, 3751. (d) Reger, D. L.; Semeniuc, R. F.; Smith, M. D. *J. Chem. Soc., Dalton Trans.* **2003**, 285. (e) Reger, D. L.; Semeniuc, R. F.; Smith, M. D. *J. Organomet. Chem.* **2003**, *666*, 87. (f) Reger, D. L.; Brown, K. J.; Smith, M. D. *J. Organomet. Chem.* **2002**, *658*, 50. (g) Reger, D. L.; Semeniuc, R. F.; Smith, M. D. *Eur. J. Inorg. Chem.* **2002**, 543. (h) Reger, D. L.; Semeniuc, R. F.; Smith, M. D. *J. Chem. Soc., Dalton Trans.* **2002**, 476. (i) Reger, D. L.; Semeniuc, R. F.; Smith, M. D. *Inorg. Chem.* **2001**, *40*, 6545.
(4) Reger, D. L.; Brown, K. J.; Gardinier, J. R.; Smith, M. D. *Organometallics* **2003**, *22*, 4973.
(5) (a) Reger, D. L.; Gardinier, J. R.; Semeniuc, R. F.; Smith, M. D. *J. Chem. Soc., Dalton Trans.* **2003**, 1712. (b) Reger, D. L.; Watson, R. P.; Gardinier, J. R.; Smith, M. D. *Inorg. Chem.* **2004**, *43*, 6609.
(6) Reger, D. L.; Gardinier, J. R.; Smith, M. D.; Shahin, A. M.; Long, G. J.; Rebbouh, L.; Grandjean, F. *Inorg. Chem.*, in press.
(7) (a) Guionneau, P.; Létard, J.-F.; Yufit, D. S.; Chasseau, D.; Bravic, G.; Goeta, A. E.; Howard, J. A. K.; Kahn, O *J. Mater. Chem.* **1999**, *9*, 985. (b) Hostettler, M.; Törnroos, K. W.; Chernyshov, D.; Vangdal, B.; Bürgi, H.-B. *Angew. Chem., Int. Ed. Engl.* **2004**, *43*, 4589.

capable of supporting supramolecular structures. We anticipated that substitution on the phenyl ring should have negligible impact on the electronic environment of the iron(II) spin state because of the sp^3 hybridization of boron and the remote location of the added substituents from the iron(II) center. Therefore, any change in the iron(II) electronic spin-state behavior would most likely be a result of changes in the crystal packing.

Faller and White[8] have shown in the 1980s that the bromine in the related cobalt(II) complex, Co[(*p*-BrC_6H_4)$B(pz)_3]_2$, could be replaced with lithium and, subsequently, with either hydrogen or deuterium by a lithium exchange reaction with butyllithium followed by hydrolysis. They also reported the acid and ester derivatives. To our knowledge, this report is the only demonstration to date of the reactivity of this functionalized poly(pyrazolyl)borate ligand in any metal complex.

We have examined alternative reactions for the related iron(II) iodides, Fe[(*p*-IC_6H_4)$B(pz)_3]_2$, **1a**, and Fe[(*p*-IC_6H_4)$B(3\text{-}Mepz)_3]_2$, **1b**. Sonogashira coupling reactions between terminal alkynes and aryl halides have been known[9] since the 1970s and have recently been used[10] to prepare complexes with spectacular architectures. Such reactions have also been used to connect organometallic and metalorganic species, such as ruthenium polypyridyls[11a] or acetylacetonates[11b] as well as metal porphyrins.[11c] We have found it remarkable that similar reactions involving tris(pyrazolyl)borates have not been explored.[11d] In this contribution we will demonstrate the utility of this reaction to derivatize Fe[(*p*-IC_6H_4)$B(3\text{-}Rpz)_3]_2$ and show how the distal substituents can be used to alter the electronic spin-state crossover behavior of the resultant iron(II) complex. We will also introduce the term "third generation" poly(pyrazolyl)borate and poly(pyrazolyl)methane ligands to designate ligands that are specifically functionalized at the noncoordinating, "back" position.

Experimental Section

General Considerations. All operations, unless otherwise specified, were carried out under a nitrogen atmosphere by using either standard Schlenk techniques or a Vacuum Atmospheres HE-493 inert atmosphere drybox. Solvents for synthetic procedures and spectroscopic studies were dried by conventional methods and distilled under a dry N_2 atmosphere immediately prior to use. All chemicals were purchased from Aldrich Chemicals. The Fe[(*p*-IC_6H_4)$B(pz)_3]_2$, **1a**, and Fe[(*p*-IC_6H_4)$B(3\text{-}Mepz)_3]_2$, **1b**, complexes were prepared as described elsewhere.[6]

Robertson Microlit Laboratories performed all elemental analyses. Melting point determinations were made on samples contained in glass capillaries by using an Electrothermal 9100 apparatus and are uncorrected. Mass spectrometric measurements, obtained in the ESI(±) mode, were obtained on a Micromass Q-Tof spectrometer, whereas those obtained by using direct probe analyses were made on a VG 70S instrument. NMR spectra were recorded, as is noted within the text, by using either a Varian Gemini 300 or a Varian Mercury 400 spectrometer. Chemical shifts were referenced to solvent resonances at δ_H 7.27 and δ_C 77.23 for $CDCl_3$.

Magnetic susceptibilities were measured at 0.5 T with a Quantum Design MPMS XL SQUID magnetometer. Gelatin capsules were used as sample containers for measurements taken in the temperature range of 5 to 300 or 350 K. The very small diamagnetic contribution of the gelatin capsule had a negligible contribution to the overall magnetization, which was dominated by the sample. The molar magnetic susceptibilities were corrected for the diamagnetism of the complexes; the corrections, which were calculated from tables of Pascal's constants, are -485×10^{-6} emu/mol for Fe[(*p*-$PhC_2C_6H_4$)$B(3\text{-}Mepz)_3]_2$, -516×10^{-6} emu/mol for Fe[(*p*-$Me_3SiC_2C_6H_4$)$B(3\text{-}Mepz)_3]_2$, and -393×10^{-6} emu/mol for Fe[(*p*-$HC_2C_6H_4$)$B(3\text{-}Mepz)_3]_2$.

The Mössbauer spectral absorber contained ca. 50 mg/cm^2 of powder mixed with boron nitride, and the spectra were measured on constant-acceleration spectrometers all of which utilized a room-temperature rhodium matrix cobalt-57 source and were calibrated at room temperature with α-iron foil. Except as noted in the tables below, the estimated absolute errors are ±0.005 mm/s for the isomer shifts, ±0.01 mm/s for the quadrupole splittings and line widths, and ±0.2% for the relative spectral absorption areas. The relative errors are estimated to be approximately one-half the above absolute errors.

General Procedure for the Alkyne Coupling Reactions with Fe[(*p*-IC_6H_4)$B(3\text{-}Rpz)_3]_2$. A Schlenk flask is charged with the desired Fe[(*p*-IC_6H_4)$B(3\text{-}Rpz)_3]_2$ complex, $Pd(PPh_3)_2Cl_2$, the desired terminal XC_2H alkyne, THF, and piperidine (ca. 20 mL, 3:1 v/v). The reaction vessel and the reactants are then subjected to three freeze/pump/thaw cycles. The reaction mixture is once again frozen, and the vessel is back-filled with N_2 and CuI is added under a N_2 atmosphere. After the reaction flask is sealed with a septum reinforced by copper wire, it is again frozen, evacuated, back-filled with nitrogen, and then placed in a 60 °C bath overnight. Then, the product mixture is adsorbed onto neutral alumina, the solvent is evaporated, and the alumina is added to a pad of fresh neutral alumina. Elution with hexanes eliminates any excess alkyne reactant and homocoupled alkynyl impurities. Finally, elution with CH_2Cl_2 yields the desired alkynylphenyl borate complex, Fe[(*p*-$XC_2C_6H_4$)$B(3\text{-}Rpz)_3]_2$, as a fast moving band (R_f ca. 0.8; purple when R = H, colorless when R = Me).

Fe[(*p*-$PhC_2C_6H_4$)$B(3\text{-}Mepz)_3]_2$, 2. This complex was prepared in 68% yield (0.158 g) by using 0.245 g (0.253 mmol) of Fe[(*p*-IC_6H_4)$B(3\text{-}Mepz)_3]_2$, 0.050 mL (0.047 g, 0.46 mmol) of HC_2Ph, 8 mg (4 mol %) of $Pd(PPh_3)_2Cl_2$, 2 mg (4 mol %) of CuI, 10 mL of THF, and 5 mL of piperidine. Crystals suitable for X-ray diffraction were grown by slow evaporation of a CH_2Cl_2 solution. Mp 345 °C dec. Anal. Calcd for $C_{40}H_{40}N_{12}B_2Fe$: C, 68.00; H, 5.27; N 18.30. Found: C, 68.23; H, 5.26; N, 18.27. ^{1}H NMR (300 MHz, $CDCl_3$) all br s: 46.03, 44.11, 8.70, 6.58 (m), 6.07, 4.25, 2.00, −5.96. Accurate ESI(+) MS: calcd for M^+, 918.3678; found, 918.3701.

Fe[(*p*-$Me_3SiC_2C_6H_4$)$B(pz)_3]_2$, 3a. This complex was prepared in 79% yield (0.232 g) as a red-orange solid by using 0.314 g (0.354 mmol) of Fe[(*p*-IC_6H_4)$B(pz)_3]_2$, 0.5 mL (0.355 g, 3.61 mmol) of HC_2SiMe_3, 22 mg (11 mol %) of $Pd(PPh_3)_2Cl_2$, 10 mg (15 mol %) of CuI, 8 mL of THF, and 8 mL of piperidine. ^{1}H NMR (300 MHz, $CDCl_3$) 8.15 (part of AA′BB′, J = 8 Hz, 4 H), 7.85 (d, J = 1 Hz, 6 H, H_3-pz), 7.72 (part of AA′BB′, J = 8 Hz, 4 H), 7.01 (br s, 6 H, H_3-pz), 6.25 (br s, 6H, H_4-pz), 0.33 (s, 9 H, $SiCH_3$). ^{13}C NMR (75.4 MHz, $CDCl_3$) 149.8, 138.6, 135.0, 131.6, 122.9, 106.8 (C_4-pz), 95.0, 89.9, 0.3 ($SiCH_3$). Accurate ESI(+) MS: calcd for M^+, 826.2901; found, 826.2894.

Fe[(*p*-$Me_3SiC_2C_6H_4$)$B(3\text{-}Mepz)_3]_2$, 3b. This complex was prepared in 81% yield (0.460 g) by using 0.609 g (0.628 mmol) of Fe[(*p*-IC_6H_4)$B(3\text{-}Mepz)_3]_2$, 1.0 mL (0.71 g, 7.2 mmol) of HC_2SiMe_3, 16 mg (4 mol %) of $Pd(PPh_3)_2Cl_2$, 3 mg (3 mol %) of CuI, 30 mL of THF, and 5 mL of piperidine. Mp 325−330 °C dec. Anal. Calcd for $C_{46}H_{56}N_{12}B_2FeSi_2$: C, 60.67; H, 6.20; N, 18.46. Found: C, 60.30; H, 6.10; N, 18.35. ^{1}H NMR (300 MHz, $CDCl_3$) all br s: 45.85, 43.49,

(8) White, D.; Faller, J. W. *J. Am. Chem. Soc.* **1982**, *104*, 1548.
(9) Sonogashira, K.; Tohda, Y.; Hagihara, N. *Tetrahedron Lett.* **1975**, 4467.
(10) (a) Laskoski, M.; Steffen, W.; Morton, J. G. M.; Smith, M. D.; Bunz, U. H. F. *Angew. Chem., Int. Ed.* **2002**, *41*, 2378. (b) Bunz, U. H. F. *Chem. Rev.* **2000**, *100*, 1605.
(11) (a) Harriman, A.; Ziessel, R. *J. Chem. Soc., Chem. Commun.* **1996**, 1707 and references therein. (b) Hoshino, Y.; Higuchi, S.; Fiedler, J.; Su, C.-Y.; Knödler, A.; Schwerderski, B.; Sarkar, B.; Hartmann, H.; Kaim, W. *Angew. Chem., Int. Ed.* **2003**, *42*, 674 and references therein. (c) Wagner, R. W.; Lindsey, J. S. *J. Am. Chem. Soc.* **1994**, *116*, 9759. (d) A pyrazabole polymer has been constructed via this methodology; see Matsumoto, F.; Chujo, Y. *Macromolecules* **2003**, *36*, 5516.

Table 1. Structural Refinements for the Fe[(*p*-X-$C_2C_6H_4$)B(3-Mepz)$_3$]$_2$ Complexes

X =	Ph, **2**	$SiMe_3$, **3b**	H, **4b**	H, **4b**	H, **4b**
empirical formula	$C_{52}H_{48}B_2FeN_{12}$	$C_{46}H_{56}B_2FeN_{12}Si_2$	$C_{40}H_{40}B_2Fe\ N_{12}$	$C_{40}H_{40}B_2Fe\ N_{12}$	$C_{40}H_{40}B_2Fe\ N_{12}$
formula weight	918.49	910.68	766.31	766.31	766.31
temperature, K	294(1)	200(1)	90(1)	150(1)	294(1)
crystal system	monoclinic	monoclinic	monoclinic	monoclinic	monoclinic
space group	*C*2/*c*	$P2_1/c$	*P*2/*c*	*P*2/*c*	*P*2/*c*
unit cell					
a, Å	25.9570(12)	15.2970(9)	18.7923(10)	19.1932(10)	19.2722(10)
b, Å	10.0679(5)	11.9528(7)	10.1073(5)	10.1436(5)	10.1801(5)
c, Å	21.0622(10)	14.1961(8)	19.8578(10)	19.6711(10)	20.1124(10)
β, deg	120.6730(10)	97.6590(10)	94.9870(10)	93.8120(10)	92.9950(10)
V, Å^3	4734.2(4)	2572.5(3)	3757.5(3)	3821.3(3)	3940.5(3)
Z	4	2	4	4	4
ρ (calcd), g cm^{-3}	1.289	1.176	1.355	1.332	1.292
abs. coeff., mm^{-1}	0.369	0.383	0.450	0.442	0.429
R1 [$I > 2\sigma(I)$]	0.0443	0.0638	0.0382	0.0396	0.0446
wR2	0.1009	0.1672	0.0963	0.1036	0.1156
R indices (all data)					
R1	0.0617	0.0849	0.0448	0.0471	0.0619
wR2	0.1064	0.1803	0.1008	0.1093	0.1270

4.27, 1.94, −1.00 ($SiMe_3$), −5.99. Accurate ESI(+) MS: calcd for M^+, 910.3842; found, 910.3831.

Fe[(*p*-$HC_2C_6H_4$)B(pz)$_3$]$_2$, 4a. A mixture of a 0.207 g (0.250 mmol) sample of Fe[(*p*-$Me_3SiC_2C_6H_4$)B(pz)$_3$]$_2$ and 50 mg (0.861 mmol) of KF in 25 mL of 50% MeOH/THF was stirred for 12 h at room temperature and then for 4 h at 60 °C (heated with an external water bath). The residue, after solvent evaporation, was passed through an alumina column with CH_2Cl_2 to yield 0.135 g (79%) of the desired complex as a red-purple solid. Mp 325 °C dec. Anal. Calcd for $C_{34}H_{28}N_{12}B_2Fe$: C, 59.87; H, 4.14; N, 24.64. Found: C, 60.13; H, 4.27; N, 24.47. ^{1}H NMR (300 MHz, $CDCl_3$) 8.29 (part of AA′BB′, 4 H), 7.79 (part of AA′BB′, 4 H), 7.73 (d, $J = 1$ Hz, 6 H, H_3-pz), 6.56 (br s, 6 H, H_3-pz), 6.12 (br s, 6H, H_4-pz), 3.22 (s, 2 H, H−C_2). Accurate ESI(+) MS: calcd For M^+, 682.2108; found, 682.2086.

Fe[(*p*-$HC_2C_6H_4$)B(3-Mepz)$_3$]$_2$, 4b. A mixture of 0.453 g (0.497 mmol) of Fe[(*p*-$Me_3SiC_2C_6H_4$)B(3-Mepz)$_3$]$_2$ and 0.106 g (1.82 mmol) of KF in 40 mL of 50% MeOH/THF was stirred for 12 h at room temperature and then for 4 h at 60 °C (heated with an external water bath). The mixture was poured into 100 mL of H_2O, and the aqueous phase was extracted with three 100 mL portions of CH_2Cl_2 followed by one 100 mL portion of Et_2O. The combined organics were dried over $MgSO_4$ and filtered, and the solvent was removed to yield 0.320 g (97%) of the desired complex as a colorless solid. This solid was recrystallized by slow diffusion of MeOH into a CH_2Cl_2 solution to give lustrous pale purple needles. Mp ca. 70 °C crystals are colorless; 285 °C dec. Anal. Calcd for $C_{40}H_{40}N_{12}B_2Fe$: C, 62.70; H, 5.26; N, 21.93. Found: C, 62.51; H, 5.29; N, 22.00. ^{1}H NMR (300 MHz, $CDCl_3$) all br s: 45.86, 43.44, 4.35, 1.94, 1.10 (C_2H), −5.99. Accurate ESI(+) MS: calcd for M^+, 766.3049; found, 766.3071.

Crystallography. X-ray intensity data were measured at 294(1) K on a colorless block shaped crystal of **2**, at 200(1) K on a colorless plate of **3b**, at 90(1), 150(1), and 294(1) K on a purple block-shaped crystal of **4b** on a Bruker SMART APEX CCD-based diffractometer (Mo Kα radiation, $\lambda = 0.710\ 73$ Å).[12] Raw data frame integration and Lp corrections were performed with SAINT+.[12] Final unit-cell parameters were determined by least-squares refinement of 6527 reflections from the data set of **2**, of 6143 reflections from the data set of **3b**, and of 7699, 7844, and 8077 reflections from the data sets of **4b** at 90, 150, and 294 K, respectively, each with $I > 5\sigma(I)$. Analysis of the data showed negligible crystal decay during data collection, and the resulting data were not corrected for absorption. Direct methods structure solution, difference Fourier calculations, and full-matrix least-squares refinement against F^2 were performed with SHELXTL.[13] Except where specified for **3b**, all non-hydrogen atoms were refined with anisotropic displacement parameters, and all hydrogen atoms were placed in geometrically idealized positions and included as riding atoms. Notes regarding the structure solution and refinement for each structure are collected below, and the numerical results are given in Table 1.

Complex **2** crystallizes in the *C*2/*c* space group as determined by the pattern of systematic absences in the intensity data and by the successful solution and refinement of the structure. The molecule resides on a 2-fold rotational axis.

Complex **3b** crystallizes in the $P2_1/c$ space group as determined uniquely by the pattern of systematic absences in the intensity data. The molecule resides on a crystallographic inversion center. The Fe[B(3-Mepz)$_3$]$_2$ core of the complex is crystallographically well ordered, but the −$C_6H_4C{\equiv}CSiMe_3$ substituent suffers from disorder which is evident in the phenyl ring, a disorder that becomes more severe further from the core of the molecule. Several unsuccessful disorder models were evaluated, and eventually it was concluded that more spatially distinct orientations are present than can be reasonably modeled from the X-ray data. In the final refinement, a model using two Si positions separated by 0.27 Å with two associated methyl group rotational orientations was employed in the fixed ratio of 0.65 to 0.35; the Si atoms were refined with common displacement parameters. The inflated displacement parameters of atoms at the $SiMe_3$ end of the molecule and the high R-factors obtained for the final structure reflect the limitations of this disorder model. Atomic positional parameters reported for these disordered atoms are therefore less precise and should be regarded as approximate. All the non-hydrogen atoms were refined with anisotropic displacement parameters except for an isotropic refinement of the minor $SiMe_3$ component.

Complex **4b** crystallizes in the *P*2/*c* space group as determined by the pattern of systematic absences in the intensity data and by the successful solution and refinement of the structure.

Results

Syntheses. The Fe[(*p*-IC_6H_4)B(pz)$_3$]$_2$, **1a**, and Fe[(*p*-IC_6H_4)B-(3-Mepz)$_3$]$_2$, **1b**, complexes were prepared in high yield by the metathetical reaction between Na[(*p*-IC_6H_4)B(3-Rpz)$_3$] and iron(II) halides as reported elsewhere.[6] These complexes successfully undergo Sonogashira coupling reactions with either phenylacetylene or trimethylsilylacetylene to produce the dialkynylated derivatives shown in Scheme 1 in good yields. The

(12) *SMART*, version 5.625, *SAINT+*, version 6.22, and *SADABS*, version 2.05; Bruker Analytical X-ray Systems, Inc.: Madison, Wisconsin, USA, 2001.

(13) Sheldrick, G. M. *SHELXTL*, version 6.1; Bruker Analytical X-ray Systems, Inc.: Madison, Wisconsin, USA, 2000.

Scheme 1. Preparation of Alkynylated Aryltris(pyrazolyl)boratoiron(II) Complexes

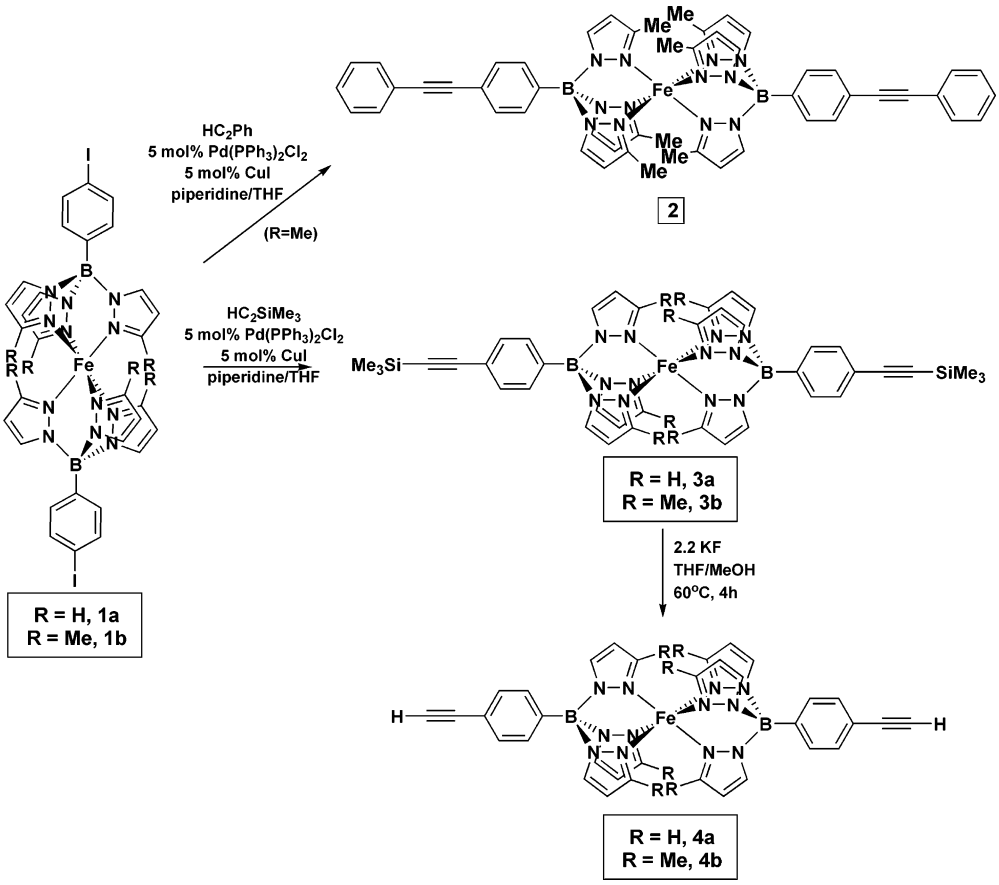

terminal dialkynyl derivatives, **4a** and **4b**, were prepared by deprotecting the trimethylsilyl derivatives with KF in hot MeOH/THF. The compounds are air stable as solids and in solution, but solutions need to be protected from light because they turn orange (presumably iron(III)). The identity of each complex has been established by a combination of elemental analyses, NMR and Mössbauer spectroscopy, mass spectrometry, and, for complexes **2**, **3b**, and **4b**, by single-crystal X-ray diffraction.

The unsubstituted pyrazolyl derivatives are purple, which greatly facilitates both separation and characterization, whereas the as-formed powders of complexes with 3-methylpyrazolyl substitution are colorless at room temperature. Compound **4b** is unique compared to **2** and **3b** in that it is pale purple in the *crystalline state*, whereas the other two remain colorless when crystalline. The color of the solid is a good indication of the spin state of the iron(II) in a poly(pyrazolyl)borate complex because a low-spin complex is purple, whereas a high-spin complex is colorless. It has been clearly established previously that interligand steric repulsions between the 3-position methyl groups in $Fe[HB(3,5\text{-}Me_2pz)_3]_2$ and related compounds such as $\{Fe[HC(3,5\text{-}Me_2pz)_3]_2\}(BF_4)_2$ favor the high-spin state that typically has Fe−N bond distances that are 0.2 Å longer than those in the low-spin state.[14] For example, even in the high-spin state $\{Fe[HC(3,5\text{-}Me_2pz)_3]_2\}(BF_4)_2$ has C···C nonbonding distances between adjacent interligand 3-methyl groups that average 3.75 Å,[14a] a value which is less than the 4.0 Å sum of the van der Waals radii of two methyl groups.[15]

NMR. As alluded to above, the unsubstituted pyrazolyl derivatives contain low-spin iron(II) and thus are diamagnetic at room temperature, and as a consequence, in solution their NMR spectra show the expected resonances with chemical shifts in the typical ranges of 1 to 10 ppm. In contrast, all the 3-methylpyrazolyl derivatives contain high-spin iron(II) and thus are paramagnetic at room temperature, and as a consequence, in solution their resonances occur over a much larger range with chemical shifts of ca. 46 to −6 ppm. The broad resonances at ca. δ_H 45.9, 43.5, 4.3, 1.9, and −6.0 ppm appear to be characteristic of the $Fe[(C_6H_4)B(3\text{-}Mepz)_3]_2$ core; however, their specific assignments remain unclear.

Magnetic Studies. The electronic spin-state crossover behavior of crystalline samples of $Fe[(p\text{-}PhC_2C_6H_4)B(3\text{-}Mepz)_3]_2$, **2**, $Fe[(p\text{-}Me_3SiC_2C_6H_4)B(3\text{-}Mepz)_3]_2$, **3b**, and $Fe[(p\text{-}HC_2C_6H_4)B(3\text{-}Mepz)_3]_2$, **4b**, has been determined by SQUID magnetometry, and the temperature dependence of both the inverse molar magnetic susceptibilities and the effective magnetic moments, μ_{eff}, obtained between 4 and 300 or 350 K upon the initial cooling, blue, and subsequent warming, red, is shown in Figure 1 (additional cooling and warming measurements superimpose on the data shown in Figure 1). As was the case for earlier studies[2e,14,17,23] of related complexes, each of these complexes exhibits interesting magnetic properties that differ significantly

(14) (a) Reger, D. L.; Little, C. A.; Rheingold, A. L.; Lam, M.; Liable-Sands, L. M.; Rhagitan, B.; Concolino, T.; Mohan, A.; Long, G. J.; Briois, V.; Grandjean, F. *Inorg. Chem.* **2001**, *40*, 1508. (b) Sohrin, Y.; Kokusen, H.; Matsui, M. *Inorg. Chem.* **1995**, *34*, 3928.

(15) (a) Bondi, A. *J. Phys. Chem.* **1964**, *68*, 441. (b) Rowland, R. S.; Taylor, R. *J. Phys. Chem.* **1996**, *100*, 738.

(16) Figgis, B. N. *Introduction to Ligand Fields*; Wiley-Interscience: New York, 1966; p 274.

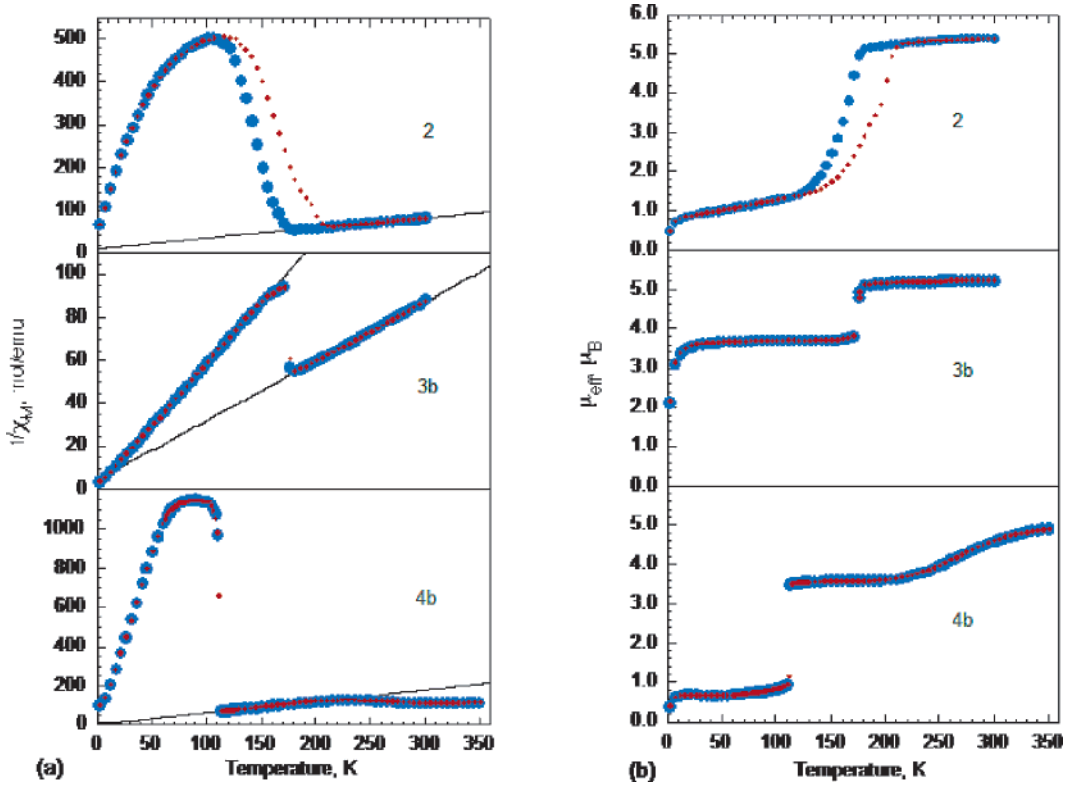

Figure 1. Temperature dependence of the inverse molar magnetic susceptibility (a) and the effective magnetic moment (b) of Fe[(*p*-$PhC_2C_6H_4$)B(3-Mepz)$_3$]$_2$, **2**, Fe[(*p*-$Me_3SiC_2C_6H_4$)B(3-Mepz)$_3$]$_2$, **3b**, and Fe[(*p*-$HC_2C_6H_4$)B(3-Mepz)$_3$]$_2$, **4b**. The results of the initial cooling of the sample are shown in blue, and the results of the initial warming are shown in red.

from those of the Fe[(*p*-IC_6H_4)B(3-Mepz)$_3$]$_2$ starting material. Thus, it is clear that changing the substituent at the 4-position of the phenyl ring can have a profound effect on the electronic spin state and, thus, on the magnetic behavior of the remote iron(II) ion.

At 294 K bulk crystalline samples exhibit magnetic moments of 5.4 and 5.2 μ_B for Fe[(*p*-$PhC_2C_6H_4$)B(3-Mepz)$_3$]$_2$, **2**, and Fe[(*p*-$Me_3SiC_2C_6H_4$)B(3-Mepz)$_3$]$_2$, **3b**, respectively. These moments are somewhat higher than the spin-only moment of 4.9 μ_B expected for a high-spin iron(II) complex and indicate the expected[16] presence of an orbital contribution to the magnetic moment. These moments are also in excellent agreement both with the ca. 5.2 μ_B moments observed at 294 K for the different polymorphs of Fe[(*p*-IC_6H_4)B(3-Mepz)$_3$]$_2$ and the moments observed in related high-spin iron(II) complexes.[17] In contrast, the moment of 4.6 μ_B observed at 294 K for crystalline Fe[(*p*-$HC_2C_6H_4$)B(3-Mepz)$_3$]$_2$, **4b**, is somewhat below the spin-only value and indicates the presence of an admixture of both the paramagnetic high-spin and diamagnetic low-spin states of iron(II), a mixture which is indicated both by the Mössbauer spectral results (vide infra) and by the color of the *crystals* of **4b** which are pale purple at room temperature; in contrast, the crystals of **2** and **3b** are colorless at room temperature.

Upon cooling, the effective magnetic moment of Fe[(*p*-$PhC_2C_6H_4$)B(3-Mepz)$_3$]$_2$, **2**, exhibits a rather gradual spin-state crossover to the low-spin state with a reproducible hysteresis that is observed upon cycling between 300 and 4 K; see the top of Figure 1b. This hysteresis is expected[18] and is typical[7,19,23] of iron(II) complexes that undergo a spin crossover accompanied by a structural phase transition as is the case for **2**, which is found to shatter as it undergoes the spin crossover; see below. The 30 K hysteresis has a $T_{1/2}$ of 163 K upon cooling and a $T_{1/2}$ of 193 K upon warming. The cooling curve has a gradual transition between 181 and 136 K, whereas the warming curve has an even more gradual transition between 151 and 211 K.

In the high-spin iron(II) state between 300 and 190 K, the inverse molar magnetic susceptibility of Fe[(*p*-$PhC_2C_6H_4$)B(3-Mepz)$_3$]$_2$, **2**, decreases linearly with a Curie constant of 4.26 (emu/mol)K and an intercept of −48.6 K, a temperature which is more negative than would be expected for a dilute paramagnetic complex. The negative value is no doubt the result of an admixture of a small portion of the diamagnetic low-spin iron(II) state into the predominant high-spin iron(II) electronic state, an admixture that increases upon cooling. As a consequence, the decrease upon cooling of the molar magnetic susceptibility and the increase of the inverse susceptibility are larger than would be expected for a completely high-spin iron(II) state. This

(17) (a) Jesson, J. P.; Trofimenko, S.; Eaton, D. R. *J. Am. Chem. Soc.* **1967**, *89*, 3158. (b) Jesson, J. P.; Weiher, J. F. *J. Chem. Phys.* **1967**, *46*, 1995. (c) Jesson, J. P.; Weiher, J. F.; Trofimenko, S. *J. Chem. Phys.* **1968**, *48*, 2058. (d) Leita, B. A.; Moubaraki, B.; Murray, K. S.; Smith, J. P.; Cashion, J. D. *J. Chem. Soc., Chem. Commun.* **2004**, 156. (e) Sugiyarto, K. H.; McHale, W.-A.; Craig, D. C.; Rae, A. D.; Scudder, M. L.; Goodwin, H. A. *J. Chem. Soc., Dalton Trans.* **2003**, 2443.
(18) (a) Chernyshov, D.; Bürgi, H.-B.; Hostettler, M.; Törnroos, K. W. *Phys. Rev. B*, **2004**, *70*, 94116. (b) Chernyshov, D.; Hostettler, M.; Törnroos, K. W.; Bürgi, H.-B. *Angew. Chem., Int. Ed. Engl.* **2004**, *42*, 3825.
(19) (a) Reger, D. L.; Little, C. A.; Smith, M. D.; Rheingold, A. L.; Lam, K.-C.; Concolino, T. L.; Long, G. J.; Hermann, R. P.; Grandjean, F. *Eur. J. Inorg. Chem.* **2002**, 1190. (b) Long, G. J.; Hutchinson, B. B. *Inorg. Chem.* **1987**, *26*, 608. (c) Létard, J.-F.; Guionneau, P.; Rabardel, L.; Howard, J. A. K.; Goeta, A. E.; Chasseau, D.; Kahn, O. *Inorg. Chem.* **1998**, *37*, 4432.
(20) Long, G. J.; Baker, W. A., Jr. *J. Chem. Soc. A* **1971**, 2956.
(21) For example: (a) Ksenofontov, V.; Gaspar, A. B.; Niel, V.; Reiman, S.; Real, J. A.; Gütlich, P. *Chem.—Eur. J.* **2004**, *10*, 1291. (b) Jakobi, R.; Spiering, H.; Gütlich, P. *J. Phys. Chem. Solids* **1992**, *53*, 267.
(22) Litterst, F. J.; Amthauer, G. *Phys. Chem. Miner*. **1984**, *10*, 250.
(23) Grandjean, F.; Long, G. J.; Huchinson, B. B.; Ohlhausen, L.; Neill, P.; Holcomb, J. D. *Inorg. Chem.* **1989**, *28*, 4406.

Table 2. Mössbauer Spectral Hyperfine Parameters for Fe[(*p*-X-$C_2C_6H_4$)B(3-Mepz)$_3$]$_2$

complex	*T*, K	δ, mm/s[a]	ΔE_Q, mm/s	Γ, mm/s	area, %	assignment
Fe[(*p*-$PhC_2C_6H_4$)B(3-Mepz)$_3$]$_2$, **2**	295	1.002	3.66	0.26	100	high-spin iron(II)
	78	0.536	0.41	0.26	100	low-spin iron(II)
	4.2	0.539	0.41	0.25	100	low-spin iron(II)
Fe[(*p*-$Me_3SiC_2C_6H_4$)B(3-Mepz)$_3$]$_2$, **3b**	295	1.000	3.70	0.22	100	high-spin iron(II)
	78	1.118	3.85	0.22	50.1	high-spin iron(II)
		0.526	0.46	0.22	49.9	low-spin iron(II)
	4.2	1.134	3.80	0.25	48.7	high-spin iron(II)
		0.532	0.45	0.25	51.3	low-spin iron(II)
Fe[(*p*-$HC_2C_6H_4$)B(3-Mepz)$_3$]$_2$, **4b**[b]	320	0.994	−3.67	0.26	50.4	high-spin Fe(1)
	295	1.008	−3.68	0.26	50.0	high-spin Fe(1)
	260	1.030	−3.70	0.24	49.5	high-spin Fe(1)
	200	1.071	−3.74	0.23	46.6	high-spin Fe(1)
	120	1.103	−3.71	0.22	28.8	high-spin Fe(1)
		0.541	0.43	0.22	21.8	low-spin Fe(1)
		0.526	0.26	0.22	49.3	low-spin Fe(2)
	85	1.135	−3.70	0.26	0.90	high-spin Fe(1)
		0.545	0.47	0.26	49.5	low-spin Fe(1)
		0.540	0.25	0.26	49.5	low-spin Fe(2)
	60	0.540	0.45	0.23	50.0	low-spin Fe(1)
		0.553	0.28	0.23	50.0	low-spin Fe(2)
	30	0.544	0.45	0.23	50.0	low-spin Fe(1)
		0.553	0.28	0.23	50.0	low-spin Fe(2)
	4.2	0.554	0.46	0.23	50.0	low-spin Fe(1)
		0.555	0.28	0.23	50.0	low-spin Fe(2)

[a] The isomer shifts are given relative to room temperature α-iron foil. [b] The complete hyperfine parameters for **4b** are given in the Supporting Information, and the relaxation hyperfine parameters for the Fe(2) site between 320 and 200 K are given in Table 3 and in the text.

increase in the inverse susceptibility with cooling accounts for the decrease in the effective magnetic moment observed for Fe[(*p*-$PhC_2C_6H_4$)B(3-Mepz)$_3$]$_2$, **2**, between 300 and 190 K; see the top of Figure 1b.

Upon cooling Fe[(*p*-$Me_3SiC_2C_6H_4$)B(3-Mepz)$_3$]$_2$, **3b**, between 300 and 4 K, its magnetic moment decreases sharply between 176 and 171 K from 5.2 μ_B to a constant moment of 3.5 μ_B, a value that is close to the 3.7 μ_B moment expected for an ca. 50:50 mixture of the high-spin and low-spin iron(II) states with moments of 5.2 and 0.4 μ_B, respectively. A plot of $1/\chi$ versus *T* is linear both above and below the spin-state crossover; see the middle portion of Figure 1a. Below the spin-state crossover, between 4 and 150 K, $1/\chi$ is linear with a Curie constant of 1.75 (emu/mol)K, and as would be expected for a dilute paramagnetic complex, an only slightly negative intercept of −2.3 K is observed. Further, the decrease in the moment below ca. 30 K is exactly that expected[16,20] from zero-field splitting in a high-spin iron(II) complex in a distorted octahedral coordination environment. Thus the decrease in moment at the lowest temperatures is not associated with any further change in the spin state of the iron(II). Above the spin crossover, between 180 and 300 K, $1/\chi$ is again linear with a Curie constant of 3.61 (emu/mol)K and an intercept of −15.7 K. Again this rather more negative than expected temperature may indicate a small admixture of the low-spin state into the high-spin iron(II) electronic state of Fe[(*p*-$Me_3SiC_2C_6H_4$)B(3-Mepz)$_3$]$_2$, **3b**.

As is easily seen in the bottom portion of Figure 1b, the temperature dependence of the magnetic moment of Fe[(*p*-$HC_2C_6H_4$)B(3-Mepz)$_3$]$_2$, **4b**, is highly unusual. As is observed for many other complexes,[20,21] **4b** undergoes two changes in its electronic spin state, but in **4b** one change, that of Fe(2) (there are two independent iron sites in the solid-state structure of **4b** that can be identified with the magnetic changes from variable temperature structural work; vide infra) is gradual between ca. 185 and 350 K, with a $T_{1/2}$ of 280 K, whereas the second change, that of Fe(1), is abrupt occurring between 106 and 114 K. In most two-step spin-state crossover complexes, both changes are either abrupt or gradual, but **4b** is unusual in that one change is gradual and corresponds to a noncooperative spin-state transition and the second is abrupt and corresponds to a cooperative spin-state crossover.[20,21] This observation is confirmed (vide infra) by the temperature dependence of both the structural and Mössbauer spectral properties of **4b**.

Upon lowering the temperature of **4b** from 350 to 185 K, the effective magnetic moment gradually decreases from 4.9 μ_B to a constant value of 3.6 μ_B between 200 and 120 K, a value which is indicative of an approximately 50:50 admixture of the high-spin and low-spin iron(II) states, an admixture that is very similar to that observed in **3b**. This 50:50 admixture is maintained until the second spin-state crossover occurs at 114 K. At temperatures between ca. 106 and 15 K the magnetic moment is constant at ca. 0.68 μ_B, and an intercept of −0.1 K is observed. This rather large moment for a low-spin iron(II) complex arises in part, from the temperature independent paramagnetism associated with the low-spin iron(II) state and, in part, from the presence of ca. 1.0 wt % of a high-spin iron(II) or high-spin iron(III) impurity, a trace impurity that only becomes apparent when **4b** is in its low-spin diamagnetic state.

Mössbauer Spectra. The samples that were used for the magnetic study were subsequently analyzed by Mössbauer spectroscopy, and the spectra obtained for Fe[(*p*-$PhC_2C_6H_4$)B(3-Mepz)$_3$]$_2$, **2**, Fe[(*p*-$Me_3SiC_2C_6H_4$)B(3-Mepz)$_3$]$_2$, **3b**, and Fe[(*p*-$HC_2C_6H_4$)B(3-Mepz)$_3$]$_2$, **4b**, are shown in Figures 2, 3, and 4, respectively; the corresponding hyperfine parameters are given in Table 2 and Table 2S in the Supporting Information.

The spectra of Fe[(*p*-$PhC_2C_6H_4$)B(3-Mepz)$_3$]$_2$, **2**, obtained at 295, 78, and 4.2 K are consistent with the magnetic moments in that the 295 K spectrum consists of one quadrupole doublet with hyperfine parameters that are indicative of high-spin iron(II); see Figure 2. Upon cooling to 78 and 4.2 K this doublet completely vanishes and is replaced by a second doublet with parameters that are indicative of low-spin iron(II).

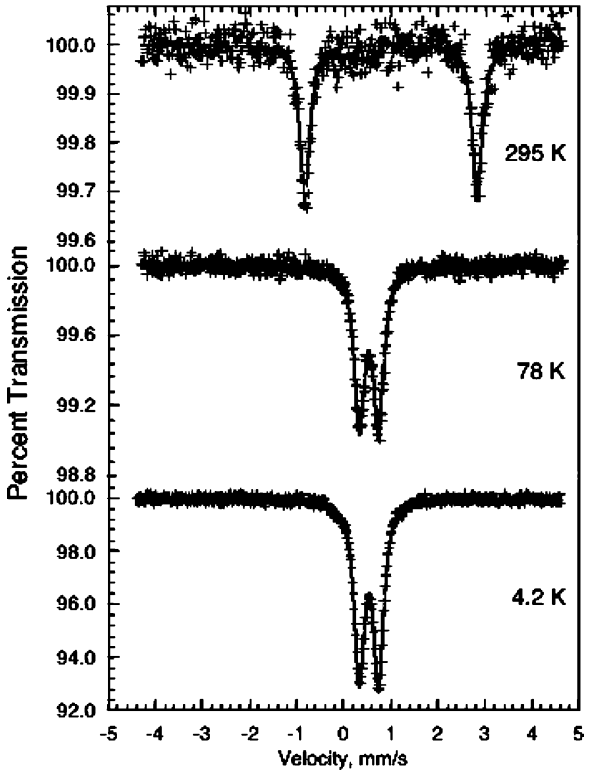

Figure 2. Mössbauer spectra of Fe[(*p*-$PhC_2C_6H_4$)B(3-Mepz)$_3$]$_2$, **2**, obtained at 295, 78, and 4.2 K.

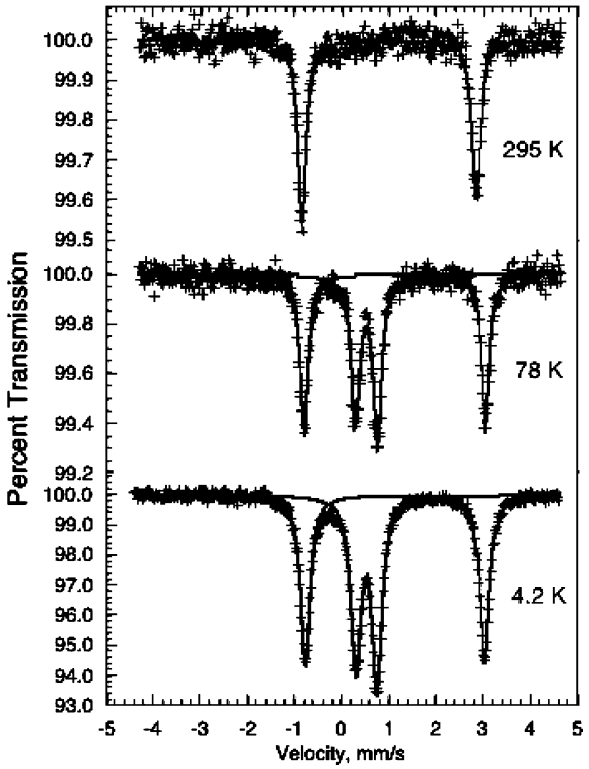

Figure 3. Mössbauer spectra of Fe[(*p*-$Me_3SiC_2C_6H_4$)B(3-Mepz)$_3$]$_2$, **3b**, obtained at 295, 78, and 4.2 K.

The Mössbauer spectra of Fe[(*p*-$Me_3SiC_2C_6H_4$)B(3-Mepz)$_3$]$_2$, **3b**, obtained at 295, 78, and 4.2 K are also consistent with the magnetic moments reported above. At 295 K the observed spectrum consists of one quadrupole doublet with hyperfine parameters that are indicative of high-spin iron(II); see Figure 3. In contrast, at 78 and 4.2 K the spectra of **3b** consist of two quadrupole doublets in a very close to 50:50 area ratio, doublets that may be assigned to high-spin and low-spin iron(II), respectively. These results are in perfect agreement with the magnetic moments that reveal a 50% spin-state crossover in **3b** at ca. 126 K.

The Mössbauer spectra observed for Fe[(*p*-$HC_2C_6H_4$)B(3-Mepz)$_3$]$_2$, **4b**, which are also fully consistent with the magnetic and structural results, are much more interesting. The spectra observed between 260 and 320 K upon heating from lower temperatures are shown in Figure 4a. The line shape of one of the spectral components observed in **4b**, assigned to the Fe(1) crystallographic site and shown in red in Figure 4a, remains high-spin, whereas the second spectral component, assigned to the Fe(2) site and shown in green, undergoes electronic spin-state relaxation between the iron(II) high-spin and low-spin states on the Mössbauer-effect time scale. As a consequence, the high-spin Fe(1) component has been fit with a quadrupole doublet, and the Fe(2) site has been fit with an electronic spin-state relaxation profile based on the method of Litterst and Amthauer.[22]

In the relaxation fits (Table 3) the observed Fe(2) line profile[22] depends on the relaxation rate, λ, the population of the high-spin state, p, and the low-spin state, $100 - p$, and the limiting hyperfine parameters of the high-spin state at high temperature and the low-spin state at low temperature. In the fits shown in Figure 4a the relaxation rate and the populations of the spin states have been adjusted, and it was found that the best fits could be obtained with constant values of 0.980 and 0.531 mm/s for the isomer shifts and -3.66 and 0.30 mm/s for the quadrupole splittings of the Fe(2) limiting high-spin and low-spin parameters, respectively; the line width was held constant at 0.23 mm/s for all the relaxation fits. Surprisingly, all attempts to introduce a temperature dependence to the four limiting hyperfine parameters were unsuccessful, and further, fits with a high-spin quadrupole splitting of $+3.66$ mm/s were totally unsuccessful, indicating that the signs of the quadrupole splittings of the high- and low-spin states of Fe(2) must be different; a similar difference was observed earlier[14a] for {Fe[$HC(pz)_3$]$_2$}(BF_4)$_2$.

An Arrhenius plot of the logarithm of the relaxation rate, λ, obtained between 260 and 320 K for **4b** is shown in Figure 5. The resulting linear Arrhenius plot yields an activation energy for the Fe(2) electronic spin-state relaxation of 1590 ± 30 cm^{-1}, a value which is typical of such relaxation processes and is similar to the energy of 1760 cm^{-1} observed[23] for the related molecular Fe[$HB(pz)_3$]$_2$ complex but is smaller that the 2820 cm^{-1} observed[14a] for the ionic {Fe[$HC(pz)_3$]$_2$}(BF_4)$_2$ complex. The corresponding high-spin populations obtained for the relaxing Fe(2) site, as well as that of the nonrelaxing Fe(1) site, are shown in Figure 6. The increase in the high-spin iron(II) population of Fe(2) between 200 and 320 K is in agreement with the gradual increase in the effective magnetic moment observed between 200 and 350 K for **4b** (see Figure 1), and the populations given in Table 3, when combined with the moments of Figure 1, are consistent with a high-spin moment of 5.12 μ_B and a low-spin moment of 0.4 μ_B. An extrapolation of the total population of the high-spin state to higher temperatures indicates that **4b** would be fully high-spin at 380 K and above; see Figure 6.

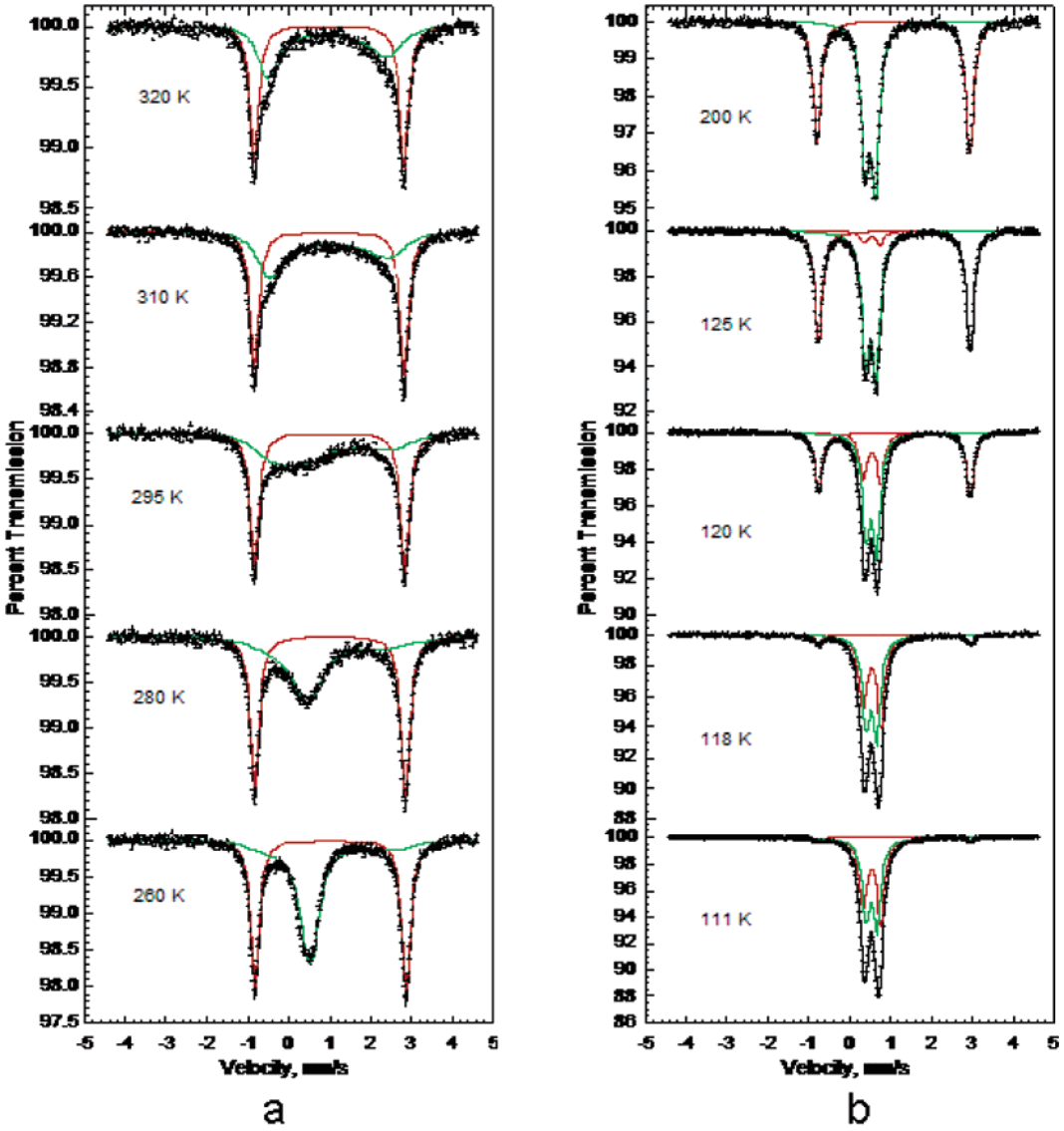

Figure 4. Mössbauer spectra of Fe[(*p*-$HC_2C_6H_4$)B(3-Mepz)$_3$]$_2$, **4b**, obtained upon heating between 260 and 320 K (a) and upon cooling between 200 and 111 K (b). The components assigned to Fe(1) are shown in red, the components assigned to Fe(2) are shown in green, and the total fits are shown in black.

Table 3. Mössbauer Spectral Relaxation Parameters for the Fe(2) Site in Fe[(*p*-$HC_2C_6H_4$)B(3-Mepz)$_3$]$_2$, **4b**

T, K	λ, mm/s	λ, MHz	ln λ	*p*, %
320	2.57(8)	29.9	0.95	63
310	1.95(8)	22.6	0.67	60
300	1.31(7)	15.2	0.27	54
295	1.18(7)	13.7	0.16	51
290	1.05(6)	12.2	0.047	48
285	0.94(6)	10.9	−0.06	45
280	0.89(5)	10.3	−0.12	41
270	0.73(4)	8.45	−0.32	38
260	0.46(3)	5.33	−0.79	32
250	0.32(2)	3.68	−1.15	28
225	0.15(1)	1.68	−1.93	14
200	0.030(5)	0.325	−3.58	2

As would be expected from the constant magnetic moment observed between 125 and 200 K, the Mössbauer spectra of **4b** show rather little change between these temperatures and indicate the presence of both the high-spin and low-spin iron(II) states in an essentially 50:50 area ratio; see Figure 6. However upon further cooling **4b** to 130 K and below, a reasonably sharp cooperative electronic spin-state crossover occurs for the Fe(1) site such that, at ca. 110 K and below, **4b** is fully low spin. At these lower temperatures it is apparent that the low-spin iron(II) hyperfine parameters for Fe(1) and Fe(2) are not the same because two low-spin quadrupole doublets are required to fit the inner spectral components. The difference is expected because the two crystallographic iron(II) sites in **4b** have slightly different local coordination environments as is indicated by the 90 K X-ray structural study reported below.

The temperature dependence of the quadrupole splittings is shown in Figure 7 where it has been assumed that the splitting of Fe(1) is negative as is observed for Fe(2). The temperature dependence of the quadrupole splitting of the Fe(1) site observed between 155 and 320 K is that expected of a distorted pseudooctahedral iron(II) complex, and the temperature dependence has been fit with the Ingalls' model.[24] The resulting fit, the red line in Figure 7, corresponds to a low-symmetry distortion which removes the degeneracy of the t_{2g} orbitals of Fe(1) by 1085 ± 40 cm^{-1}, a value which is somewhat high but

(24) Ingalls, R. *Phys. Rev.* **1964**, *133*, A787.

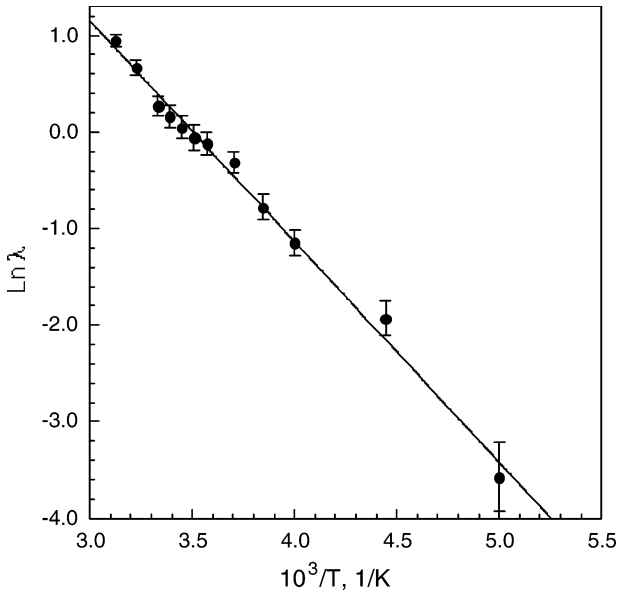

Figure 5. Arrhenius plot of the logarithm of the relaxation rate, λ, obtained between 260 and 320 K for Fe(2) in Fe[(*p*-$HC_2C_6H_4$)B(3-Mepz)$_3$]$_2$, **4b**.

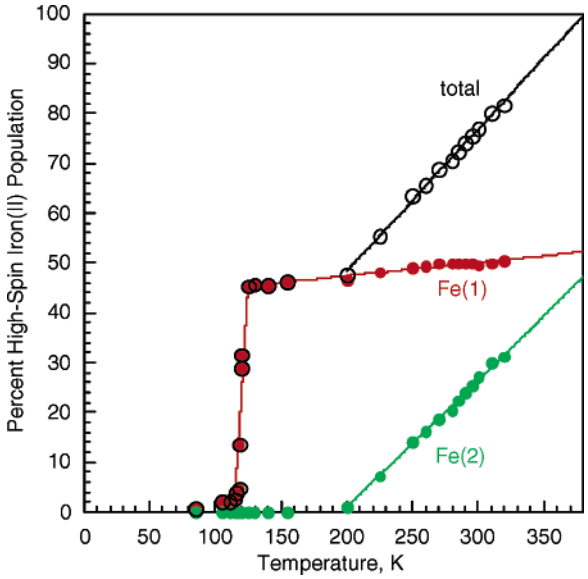

Figure 6. Temperature dependence of the high-spin population of the two iron(II) sites and their total, observed in Fe[(*p*-$HC_2C_6H_4$)B(3-Mepz)$_3$]$_2$, **4b**.

not unexpected for the highly distorted Fe(1) environment found in **4b**. The Ingalls' model assumes that there is no change in structure with temperature. This is not completely the case for either of the iron(II) sites in **4b** as is indicated by a calculation[25] of the percentage distortion in the Fe(1)−N and Fe(2)−N bond distances and the N−Fe(1)−N intraligand bond angles from the structural results presented below. For Fe(1) the percentage bond distance distortion is 0.75, 1.46, and 1.28%, and the percentage angle distortion is 0.25, 1.03, and 1.19% at 90, 150, and 294 K, respectively. So a portion of the increase in magnitude of the Fe(1) quadrupole splitting may result from the small increase in distortion in the bond distances upon cooling from 294 to 150 K. Thus the 1085 ± 40 cm^{-1} value obtained above represents the upper limit for the low-symmetry splitting of the t_{2g} orbitals of Fe(1). For Fe(2) the analogous percentage bond distance distortion is 0.61, 0.48, and 0.71%, and the percentage

(25) Renner B.; Lehmann, G. *Z. Kristallografiya* **1986**, *175*, 43.

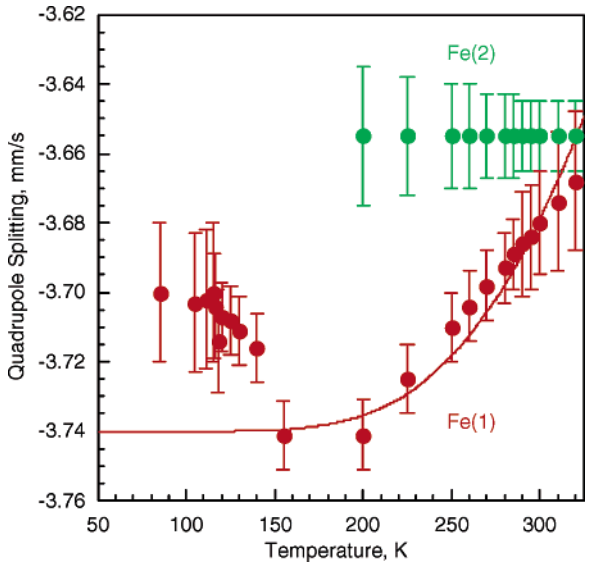

Figure 7. Temperature dependence of the quadrupole splitting of the high-spin iron(II) states in Fe[(*p*-$HC_2C_6H_4$)B(3-Mepz)$_3$]$_2$, **4b**. The solid line is a fit of the 155 to 320 K quadrupole splittings assigned to Fe(1) with the Ingalls' model; see text.

angle distortion is 0.19, 0.13, and 0.95% at 90, 150, and 294 K, respectively. Thus, on the basis of the lower percentage distortions of Fe(2) as compared with Fe(1), one would expect to observe a smaller magnitude, i.e., a less negative value, for the high-spin Fe(2) quadrupole splitting, just as is observed in the fits and shown in Figure 7.

Clearly, below 155 K the quadrupole splitting of the Fe(1) site deviates from the expected value of ca. −3.74 mm/s, a deviation that presumably results from a change in the local environment. The lattice contribution to the quadrupole splitting is likely to change as a result of the contraction of the lattice observed at 90 K, see Table 1, and because of the reduced percentage distortions at the lower temperatures. In addition, the lattice contribution usually has the opposite sign to the electronic contribution and, hence, in this case is positive. A change in the lattice contribution of only 0.04 mm/s below 150 K could account for the observed increase in the quadrupole splitting from −3.74 mm/s at 155 K to −3.70 mm/s at 85 K.

Below ca. 125 K, as the Fe(1) site begins to undergo the spin-state crossover to the low-spin state, it is necessary to use two quadrupole doublets to fit the low-spin components of the Mössbauer spectra (see Figure 4b); fits with a single low-spin quadrupole doublet are very poor. Again two doublets would be expected for the two crystallographically distinct low-spin iron(II) sites, and Fe(1) has a larger quadrupole splitting than does Fe(2) (see Table 2 and Table 2S) in agreement with the larger percentage distortions of the Fe(1) site at 90 K.

A comparison of the hyperfine parameters given in Table 2 and Table 2S indicates that, as expected, the isomer shifts for each of the high-spin or low-spin iron(II) sites are very similar; the increase observed upon cooling is perfectly normal and is a consequence of the second-order Doppler shift. In contrast, there are significant differences in the quadrupole splittings, especially for the low-spin site. Specifically, the low-spin Fe(2) site in **4b** exhibits a significantly smaller quadrupole splitting, an indication of a less distorted coordination environment in **4b** as compared to **2** and **3b**. A further comparison of the hyperfine parameters given in Table 2 and Table 2S with those

reported[6] for the various polymorphs of Fe[(*p*-IC_6H_4)B(3-Mepz)$_3$]$_2$ indicates that they are again virtually identical with the exception of the smaller high-spin quadrupole splitting observed in **4b** at 295 K. It should be noted that the quadrupole splitting of 0.32 mm/s observed[6] at 78 K for the low-spin Fe[(*p*-IC_6H_4)B(pz)$_3$]$_2$ complex is very close to the average of 0.36 mm/s observed for the two low-spin iron(II) sites in Fe[(*p*-$HC_2C_6H_4$)B(3-Mepz)$_3$]$_2$, **4b**, at 85 K.

Solid-State Structures. An analysis of the structural features of the iron(II) poly(pyrazolyl)borate complexes has provided useful indications of the spin state of the iron(II) ion. Low-spin complexes tend to have shorter iron−nitrogen bond distances of ca. 1.98 Å, whereas high-spin complexes have distances of ca. 2.19 Å as a result of the antibonding character of the partially filled e_g* orbitals in the latter case. Because the bite angles of tris(pyrazolyl)borate ligands are generally fixed, there are other subtle distortions of the ligand framework that occur on binding to metal ions of different size. We have previously noted in tris(pyrazolyl)methane iron(II) complexes that the extent of tilting of the pyrazolyl rings from the ideal C_{3v} symmetry depends on the spin state of the iron(II) ions. The MN(n1)−N(n2)C(n1) and MN(n1)−N(n2)B torsion angles, where *n* is the pyrazolyl ring number and M is a divalent metal ion (see Figure 8) describe the degree of tilting.[26] When these ligands are bound to smaller metals, e.g., low-spin iron(II), the MN−NC and MN−NB torsion angles approach their ideal values of 180° and 0°, respectively. When the ligands bind larger metals, e.g., high-spin iron(II), the MN−NC angles decrease and the MN−NB angles increase in magnitude. This tilting is best visualized in Figure 8b, which shows the two independent molecules of compound **4b** at 150 K oriented down the pseudo 3-fold axis. At this temperature, the molecule on the left, with the greater tilting, is high spin whereas the molecule on the right is low spin.

The molecular structures and atom labeling schemes for complexes **2**, **3b**, and **4b** are given in Figure 8, and selected bond distances and angles are given in Table 4. The relatively long average Fe−N bond distance of 2.172 Å and the smaller FeN−NC and larger FeN−NB average torsion angles of 164.7° and 10.5°, respectively, in the 294 K structure of Fe[(*p*-$PhC_2C_6H_4$)B(3-Mepz)$_3$]$_2$, **2**, indicate that the iron(II) is high spin. The phenyl rings in the Ph−C_2−C_6H_4 ligand fragment approach orthogonality with a dihedral angle between the respective planes of 80.09(12)°. Crystals of **2** shatter upon cooling below ca. 160 K, the onset of the spin-state crossover.

The 200 K structure of Fe[($Me_3SiC_2C_6H_4$)B(3-Mepz)$_3$]$_2$, **3b**, is afflicted with a structural disorder that was modeled as two closely positioned, but rotationally independent, $SiMe_3$ groups. This disorder model resulted in a structure of reduced accuracy, but the connectivity and general features of the Fe(pz)$_6$B$_2$ core could be established. The average Fe−N bond length is 2.165(3) Å, and the average FeN−NC and FeN−NB torsion angles are 165.4 and 7.9°, respectively, values which are indicative of high-spin iron(II). Attempts to obtain lower temperature structures of this complex were thwarted by crystal shattering that occurred at ca. 175 K, a temperature within the region where the magnetic results indicate that the spin-state crossover occurs.

The crystals of Fe[(*p*-$HC_2C_6H_4$)B(3-Mepz)$_3$]$_2$, **4b**, were stable enough that structures could be obtained at 90, 150, and 294 K, i.e., for the three magnetically distinct regions of differing electronic spin states; see Figure 1. The structure of Fe[(*p*-$HC_2C_6H_4$)B(3-Mepz)$_3$]$_2$ at each temperature contains two crystallographically independent iron(II) sites. A summary of the changes in the Fe−N bond lengths and angles, as a function of temperature, is given in Table 4. The [(*p*-$HC_2C_6H_4$)B(3-Mepz)$_3$]$^-$ ligands surrounding Fe(1) are always more distorted than those surrounding Fe(2). At 90 K the sample is deep purple and both iron sites are fully low spin as is indicated by the average Fe−N bond distances and the corresponding FeN−NC and FeN−NB torsion angles, which are 1.994 Å and 169.8° and 5.2° for Fe(1) and 1.989 Å and 172.1° and 4.8° for Fe(2). Upon heating to 150 K, the Fe(1) site undergoes a spin-state crossover and is high spin with an average Fe−N distance of 2.173 Å and Fe(1)N−NC and Fe(1)N−NB torsion angles of 163.5° and 9.3°, whereas the Fe(2) site remains low spin with

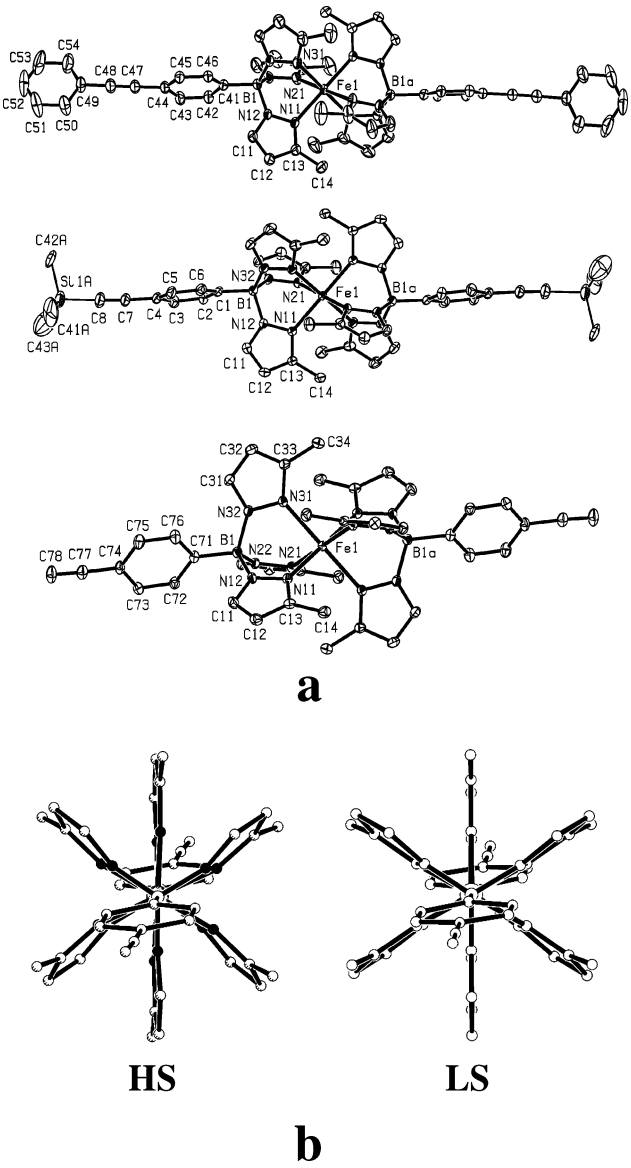

Figure 8. (a) Molecular structures and atom labeling for Fe[(*p*-$PhC_2C_6H_4$)B(3-Mepz)$_3$]$_2$, **2** (top), one disordered component of Fe[(*p*-$Me_3SiC_2C_6H_4$)B(3-Mepz)$_3$]$_2$, **3b**, and one of the two crystallographically independent Fe[(*p*-$HC_2C_6H_4$)B(3-Mepz)$_3$]$_2$, **4b**, molecules from the 90 K structure determination (bottom). (b) Two independent molecules of compound **4b** at 150 K oriented down the pseudo 3-fold axis showing the tilting of the pyrazolyl rings.

(26) Reger, D. L.; Wright, T. D.; Little, C. A.; Lamba, J. J. S.; Smith, M. D. *Inorg. Chem.* **2001**, *40*, 3810.

Table 4. Selected Bond Distances, Angles, and Torsion Angles for Fe[*p*-X-$C_2C_6H_4B$(3-Mepz)$_3$]$_2$ Complexes

X	Ph, **2**	$SiMe_3$, **3b**	H, **4b**	H, **4b**	H, **4b**
temperature (K)	294	200	90	150	294
		bond distances (Å)			
Fe(1)−N(11)	2.1316(18)	2.109(3)	1.9720(14)	2.1260(14)	2.1366(16)
Fe(1)−N(21)	2.1701(18)	2.201(3)	2.0132(13)	2.2168(14)	2.2129(16)
Fe(1)−N(31)	2.2151(19)	2.185(3)	1.9979(14)	2.1776(14)	2.1855(17)
Fe(2)−N(41)			1.9709(14)	1.9733(14)	2.0785(17)
Fe(2)−N(51)			1.9995(14)	1.9987(13)	2.1200(17)
Fe(2)−N(61)			1.9973(14)	1.9909(13)	2.1043(18)
		bond angles (deg)			
N(11)−Fe(1)−N(21)	85.52(7)	85.76(11)	90.16(5)	86.38(5)	86.05(6)
N(21)−Fe(1)−N(31)	87.81(7)	88.76(10)	89.86(5)	88.40(5)	88.43(6)
N(31)−Fe(1)−N(11)	84.81(7)	85.92(12)	90.52(6)	86.40(5)	86.14(6)
N(11a)−Fe(1)−N(11)	179.79(10)	180	180	180	180
N(21a)−Fe(1)−N(21)	91.32(10)	94.24(11)	180	180	180
N(31a)−Fe(1)−N(31)	93.08(10)	180	180	180	180
N(11)−Fe(1)−N(21a)	94.33(7)	94.24(11)	89.84(5)	93.62(5)	93.95(6)
N(21)−Fe(1)−N(31a)	178.81(7)	91.24(10)	90.14(5)	91.60(5)	91.57(6)
N(31)−Fe(1)−N(11a)	95.34(7)	94.08(12)	89.48(6)	93.60(5)	93.86(6)
N(12)−B(1)−N(22)	110.19(19)	109.9(3)	108.10(13)	109.38(13)	109.16(17)
N(22)−B(1)−N(32)	104.98(19)	104.9(3)	104.37(13)	105.11(13)	105.04(16)
N(32)−B(1)−N(12)	109.05(19)	109.5(3)	108.85(13)	110.95(14)	110.57(16)
FeN−NC average	164.7	165.4	Fe(1) 169.8	163.5	164.4
torsion			Fe(2) 172.1	172.6	170.2

an average distance of 1.988 Å and Fe(2)N−NC and Fe(2)N−NB torsion angles of 172.8° and 4.4°. Figure 8b shows these differences in torsion angles. The figure also shows a general feature of PhB(3-Rpz)3-complexes in that one pair of pyrazolyl rings, the pair oriented perpendicular to the phenyl ring, is not extensively tilted (173.8° and 179.5°, respectively), whereas the other rings are distorted, even in the low-spin case. Upon further heating to 294 K, the Fe(1) site remains high spin with an average distance of 2.178 Å and Fe(1)N−NC and Fe(1)N−NB torsion angles of 164.4° and 9.2°, whereas the Fe(2) site has an average distance of 2.101 Å and Fe(2)N−NC and Fe(2)N−NB torsion angles of 170.2° and 6.0°, values that are intermediate between those expected for low-spin and high-spin iron(II) ions. These structural results correlate well with both the magnetic and Mössbauer spectral results that indicate that the Fe(2) site in **4b** is undergoing relaxation between the high-spin and low-spin iron(II) states at 294 K.

Supramolecular Structures. Because the magnetic properties of spin-state crossover complexes depend on the packing behavior of the magnetically active metal ions, it is important to examine the supramolecular structures of the structurally characterized complexes in detail. The Fe[(*p*-$PhC_2C_6H_4$)B(3-Mepz)$_3$]$_2$ complex, **2**, has a three-dimensional supramolecular structure comprised of multiple CH−π interactions (see Figure 9) involving the $PhC_2C_6H_4$ and pyrazolyl moieties; there are no $\pi-\pi$ stacking interactions. As mentioned above, the aryl rings in the $PhC_2C_6H_4$ groups are nearly orthogonal (ca. 80° dihedral) and, therefore, possess a suitable geometry for tandem edge-to-face CH−π stacking interactions between the terminal aryl groups. In this case, the phenyl groups sandwich the C_6H_4 moieties to give sheets in the *bc*-plane as is shown at the top of Figure 9. The sheets are stacked in the third dimension as a result of CH−π interactions between pyrazolyl rings and the C_6H_4 group; see the bottom of Figure 9. There are also other CH−π interactions that help support the overall structure.

An analysis of each disorder component in the structure of Fe[(*p*-$Me_3SiC_2C_6H_4$)B(3-Mepz)$_3$]$_2$, **3b**, was undertaken for qualitative purposes, and each component exhibited the same

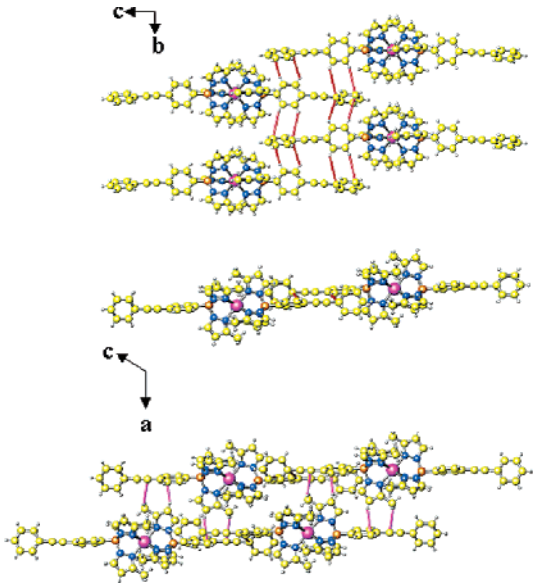

Figure 9. Supramolecular structure of Fe[(*p*-$PhC_2C_6H_4$)B(3-Mepz)$_3$]$_2$, **2**, revealing the CH−π stacking interactions that occur between phenyl rings, the red lines, and those involving pyrazolyl hydrogens, the pink lines. (Top) The CH−π interactions forming sheets in the *bc*-plane. (Middle) A side view of the sheet. (Bottom) Two sheets viewed end-on that are stacked along the *a*-axis by pz-Ph CH−π interactions, the pink lines.

two-dimensional sheet structure. The structure was organized by three CH−π interactions of less than 3.05 Å, the cutoff limit for such interactions,[27] with the phenyl ring serving as the acceptor for each of these interactions and the hydrogen donors originating from the ring and methyl group of the pyrazolyl ring containing N(12) and the disordered $SiMe_3$.

The supramolecular structure of Fe[(*p*-$HC_2C_6H_4$)B(3-Mepz)$_3$]$_2$, **4b**, observed at 90 K (see Figure 10) is unusual in that the two independent iron(II) sites are segregated into different

(27) (a) Takahashi, H.; Tsuboyama, S.; Umezawa, Y.; Honda, K.; Nishio, M. *Tetrahedron* **2000**, *56*, 6185. (b) Tsuzuki, S.; Honda, K.; Uchimaru, T.; Mikami, M.; Tanabe, K. *J. Am. Chem. Soc.* **2000**, *122*, 11450. (c) Braga, D.; Grepioni, F.; Tedesco, E. *Organometallics* **1998**, *17*, 2669.

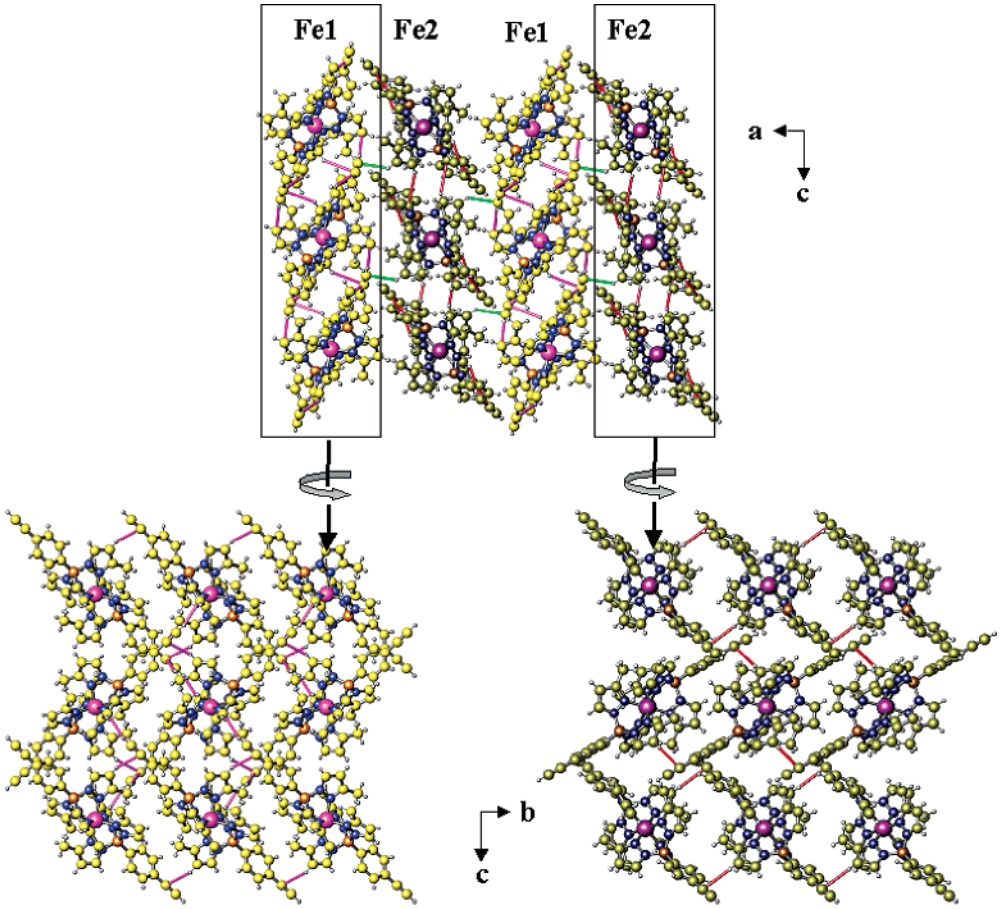

Figure 10. (Top) supramolecular structure of Fe[(*p*-$HC_2C_6H_4$)B(3-Mepz)$_3$]$_2$, **4b**, showing the alternating sheets of molecules containing Fe(1), lighter pink, and Fe(2), darker pink, that are connected via CH$-\pi$ interactions, the green lines, involving the alkynyl fragments. (Bottom) A side view of the sheets comprised of CH$-\pi$ interactions, the pink lines for Fe(1), and the red lines for Fe(2).

portions of the structure. More specifically, the overall structure is that of stacked bilayer sheets where one sheet, containing the Fe(1) ions, is alternately stacked with sheets that contain the Fe(2) ions; see the top of Figure 10. A set of CH$-\pi$ interactions involving a pyrazolyl ring hydrogen and the π-electron cloud of the alkynyl group holds the sheets together where the CH(52)$-$C(78) distance of 2.68 Å (135.3°) is the closest contact distance. The geometry of this interaction is comparable to other CH$-\pi$ (C≡C) interactions.[28]

There are other relatively close contacts, not shown in Figure 10, between CH(31)$-$C(88) at 3.01 Å (152.4°) and CH(24b)$-$C(88) at 3.03 Å (128.7°) that are just below the 3.05 Å limit for typical CH$-\pi$ interactions[27] and above the sum of the van der Waals radii for carbon and hydrogen of 2.90 Å.[15] It is therefore, likely that the CH$-\pi$ interactions weakly support the intersheet stacking. The Fe(1) sheets are held together in the *bc*-plane by two long CH$-\pi$ (C≡C) interactions.[28] The first occurs between the acidic alkynyl hydrogen and the π-electron cloud of the pyrazolyl ring containing N(21) {CH(78)$-$Ct-[N(21)] distance of 3.04 Å, angle of 147.3°, where Ct stands for the centroid of the pyrazolyl ring}, and the second occurs between the pyrazolyl methyl hydrogen and the π-electron cloud of the alkynyl group [CH(34b)$-$C(77), 3.030 Å, 144.26°]. This framework is further supported in the *b*-axis direction by a CH$-\pi$ interaction between a pyrazolyl ring hydrogen and the π-electron cloud of the alkynyl group CH(32)$-$C(77) [2.87 Å, 147.0°]. In the case of the sheets that hold the Fe(2) ions, a CH$-\pi$ interaction between a pyrazolyl ring hydrogen and the π-electron cloud of the alkyne [CH(62)$-$C(87) 2.78 Å, 165.6°] assembles the molecules into chains that run along the *b*-axis, whereas another CH$-\pi$ interaction between a pyrazolyl ring hydrogen and the phenyl group {CH(51)$-$Ct[C(81)], 2.97 Å, 137.2°} affords connectivity in the *c*-direction.

The overall stacking arrangement in Fe[(*p*-$HC_2C_6H_4$)B(3-Mepz)$_3$]$_2$, **4b**, is preserved in the structures determined at 150 and 294 K, and the geometries of the relevant noncovalent interactions are given in Table 5. Generally, as expected, the interatomic distances for noncovalent interactions increase with increasing temperature. Exceptions to this trend are those interactions that result in connectivity that is solely in the *b*-direction or within the *ab*-plane. In these cases, the interatomic distances actually decrease with increasing temperature between 90 and 150 K. Presumably, the distances at 150 K represent equilibrium distances between attractive and repulsive interactions. On further heating to 294 K, the interacting atoms are further separated.

Discussion

The efficiency of the Sonogashira coupling reactions with the aryl iodide groups in the Fe[(*p*-IC_6H_4)B(3-Rpz)$_3$]$_2$ complexes and the ease of purification of the resulting new iron(II)

(28) Lu, W.; Chan, M. C. W.; Zhu, N.; Che, C.-M.; He, Z.; Wong, K.-Y. *Chem. Eur. J.* **2003**, *9*, 6155. Steiner, T.; Tamm, M. *J. Organomet. Chem.* **1998**, *570*, 235.

Table 5. Short Contact Distances and Noncovalent Interactions in Fe[(*p*-$HC_2C_6H_4$)B(3-Mepz)$_3$]$_2$, **4b**

	d_{DH-A} Å (θ_{DHA}, deg)		
	90 K	150 K	294 K
Fe(2) Sheet			
CH(51)−Ct[C(81)]	2.973 (137.2)	2.995 (136.9)	3.098 (134.5)
[a]CH(64b)-Ct[C(81)]	3.318 (146.4)	3.296 (143.1)	3.300 (144.1)
[a]CH(62)−C(87)	2.781 (165.6)	2.768 (164.1)	2.836 (164.9)
CH(62)−C(88)	2.919 (159.4)	2.858 (162.0)	2.897 (168.8)
Fe(1) Sheet			
[a]CH(78)−Ct[N(21)]	3.043 (147.3)	2.970 (148.6)	3.170 (146.5)
CH(34b)-C(77)	3.030 (144.3)	3.207 (110.6)	3.112 (151.7)
CH(32)−C(77)	2.870 (147.0)	2.897 (152.4)	2.981 (151.7)
CH(32)−C(78)	2.913 (149.5)	2.936 (158.8)	3.013 (158.6)
Intersheet			
CH(88)−Ct[C(71)]	3.024 (111.8)	3.053 (113.5)	3.229 (111.1)
CH(52)−C(77)	2.947 (144.6)	3.011 (143.9)	3.166 (144.2)
CH(52)−C(78)	2.681 (135.3)	2.721 (134.6)	2.789 (136.4)
[b]CH(31)−C(88)	3.007 (152.4)	2.928 (159.2)	3.023 (161.1)
CH(24b)-C(88)	3.028 (128.7)	3.132 (117.9)	3.096 (124.7)

[a] Contacts in the *b*-direction. [b] Contacts in the *ab*-plane.

complexes make this synthetic method very attractive both for the derivatization of spin-state crossover complexes and for the continuing study of the relationship between supramolecular organization and the magnetic behavior of the resultant solids. Indeed, this reaction-type opens up a new direction in poly(pyrazolyl)borate chemistry, a general route to the syntheses of a new type of third generation poly(pyrazolyl)borate ligands. First generation poly(pyrazolyl)borate ligands, initially introduced by Trofimenko,[29] are the simple $[HB(Rpz)_3]^-$ type ligands with nonbulky substituents at the 3-position. Second generation ligands, also introduced by Trofimenko,[30] are those with bulky substituents at the 3-position. Third generation ligands are designed to be those specifically functionalized at the noncoordinating, "back" position of the ligands. Whereas the simple $[RB(pz)_3]^-$ type ligands have been known for many years, the Co[(*p*-BrC_6H_4)$B(pz)_3]_2$ complex and its derivatives outlined in the Introduction were the first important complexes containing third generation ligands.[8] Subsequently a few other such ligands have been prepared,[31] most notable being the boron−boron linked ligands,[31a,d] such as $[(pz)_3BB(pz)_3]^{2-}$, and the ferrocene (Fc) and phenyl linked ligands, such as $\{Fc[B(pz)_3]_2\}^{2-}$, introduced by Wagner.[32] In related chemistry, we have developed a series of third generation poly(pyrazolyl)methane ligands, such as $C_6H_{6-n}[CH_2OCH_2C(pz)_3]_n$, ($n$ = 2, 3, 4, and 6),[3] Fc-$[CH(pz)_2]_2$,[4] and $(CH_2)_m[CH(pz)_2]_2$, (m = 1−3),[5] based on linking poly(pyrazolyl)methane units into single molecules. Given that the M[(*p*-I/BrC_6H_4)$B(3\text{-}Rpz)_3]_2$ (M = Fe, Co) syntheses involve the reaction of Na[(*p*-IC_6H_4)$B(3\text{-}Rpz)_3$] (the synthesis of which is a high yield procedure) and metal halides, an appropriate M[(*p*-I/BrC_6H_4)$B(3\text{-}Rpz)_3$]-derivative of many different metal systems should be readily achievable. We anticipate that our introduction herein of this new route to derivatize metal complexes of poly(pyrazolyl)borate ligands by using Sonogashira coupling reactions (related coupling reactions are also possible) with aryl iodide groups in the M[(*p*-IC_6H_4)B-$(3\text{-}Rpz)_3$]-type complexes will open an exciting new chapter for the use of these ligands in many applications ranging from models for biological systems to components of "molecular machines."

It is generally accepted that the abruptness of the spin-state crossover is dictated by cooperative interactions between molecules or ionic complexes in the solid phase. In the current study, we prepared Fe[(*p*-$PhC_2C_6H_4$)$B(3\text{-}Mepz)_3]_2$, **2**, to take advantage of the known and relatively predictable CH−π stacking behavior of the phenylethynyl(phenyl) moieties.[33] It was found that the system packed in the expected way, and the resulting solid showed a high-spin to low-spin crossover with a hysteresis. Molecules that show hysteresis are often associated with both a significant degree of cooperativity and a crystallographic phase transition, although neither condition is sufficient to guarantee the presence of a thermal hysteresis.[18] It is likely that **2** undergoes a phase transition because the crystals shatter on cooling below the spin-state crossover temperature. It is also likely that **3b** also undergoes a phase change, as crystals of this complex shatter on cooling below its abrupt high-spin to low-spin crossover, but no hysteresis is observed. In this case, the CH−π interactions in **3b** result in only a two-dimensional supramolecular structure rather than the three-dimensional structure observed for **2**.

The magnetic behavior of **3b** is unusual in that it is an unusual example of a complex with equivalent iron(II) sites at higher temperatures that undergoes a 50% spin-state crossover; the remaining high-spin iron(II) does not change above 4 K. The first example[34] was a related tris(pyrazolyl)methane complex, $\{Fe[HC(3,5\text{-}Me_2pz)_3]_2\}(BF_4)_2$. In this complex, clear, colorless crystals of $\{Fe[HC(3,5\text{-}Me_2pz)_3]_2\}(BF_4)_2$ cooled to 173 K turn purple and undergo a phase transition from C-centered monoclinic to primitive triclinic; fortunately, the crystals do not shatter at low temperatures while undergoing the phase transition. By preparing the analogous divalent Co, Ni, and Cu complexes, which also undergo the same phase transition, but no electronic spin-state or magnetic changes, we have conclusively demonstrated that the phase transition yields the unusual partial spin-state crossover behavior in $\{Fe[HC(3,5\text{-}Me_2pz)_3]_2\}(BF_4)_2$. Specifically, the phase transition causes a decrease in the MN−NC torsion angles for only one-half of the dications in all four complexes, a distortion that favors larger metals, thus energetically preventing one-half of the iron(II) ions in {Fe[HC(3,5-

(29) Trofimenko, S. *Scorpionates − The Coordination Chemistry of Polypyrazolylborate Ligands*; Imperial College Press: London, 1999.
(30) Trofimenko, S.; Calabrese, J. C.; Thompson, J. S. *Inorg. Chem.* **1987**, *28*, 1507.
(31) (a) Brock, C. P.; Das, M. K.; Minton, R. P.; Niedenzu, K. *J. Am. Chem. Soc.* **1988**, *110*, 817. (b) Janiak, C.; Braun, L.; Girgsdies, F. *J. Chem. Soc., Dalton Trans.* **1999**, 3133. (c) Kisko, J. L.; Hascall, T.; Kimblin, C.; Parkin, G. *J. Chem. Soc., Dalton Trans.* **1999**, 1929. (d) Hardin, N. C.; Jeffery, J. C.; McCleverty, J. A.; Rees, L. H.; Ward, M. A. *New J. Chem.* **1998**, 661. (e) Niedenzu, K.; Trofimenko, S. *Inorg. Chem.* **1985**, *24*, 4222.
(32) (a) Jäkle, F.; Polborn, K.; Wagner, M. *Chem. Ber.* **1996**, *129*, 603. (b) Fabrizi de Biani, F.; Jäkle, F.; Spiegler, M.; Wagner, M.; Zanello, P. *Inorg. Chem.* **1997**, *36*, 2103. (c) Herdtweck, E.; Peters, F.; Scherer, W.; Wagner, M. *Polyhedron* **1998**, *17*, 1149. (d) Guo, S. L.; Peters, F.; Fabrizi de Biani, F.; Bats, J. W.; Herdtweck, E.; Zanello, P.; Wagner, M. *Inorg. Chem.* **2001**, *40*, 4928. (e) Guo, S. L.; Bats, J. W.; Bolte, M.; Wagner, M. *J. Chem. Soc., Dalton Trans.* **2001**, 3572. (f) Bieller, S.; Zhang, F.; Bolte, M.; Bats, J. W.; Lerner, H.-W.; Wagner, M. *Organometallics* **2004**, *23*, 2107.
(33) (a) Coates, G. W.; Dunn, A. R.; Henling, L. M.; Dougherty, D. A.; Grubbs, R. H. *Angew. Chem., Int. Ed. Engl.* **1997**, *36*, 248. (b) Coates, G. W.; Dunn, A. R.; Henling, L. M.; Ziller, J. W.; Lobkovsky, E. B.; Grubbs, R. H. *J. Am. Chem. Soc.* **1998**, *120*, 3641. (c) Weck, M.; Dunn, A. R.; Matsumoto, K.; Coates, G. W.; Lobkovsky, E. B.; Grubbs, R. H. *Angew. Chem., Int. Ed.* **1999**, *38*, 2741. (d) Lu, W.; Chan, M. C. W.; Zhu, N.; Che, C.-M.; He, Z.; Wong, K.-Y. *Chem.−Eur. J.* **2003**, *9*, 6155. (e) Shetty, A. S.; Zhang, J.; Moore, J. S. *J. Am. Chem. Soc.* **1996**, *118*, 1019. (f) Kübel, C.; Mio, M. J.; Moore, J. S.; Martin, D. C. *J. Am. Chem. Soc.* **2002**, *124*, 8605. (g) Weiss, H.-C.; Bläser, D.; Boese, R.; Doughan, B. M.; Haley, M. M. *J. Chem. Soc., Chem. Commun.* **1997**, 1703.
(34) (a) Reger, D. L.; Little, C. A.; Young, V. A., Jr.; Pink, M. *Inorg. Chem.* **2001**, *40*, 2870. (b) Reger, D. L.; Little, C. A.; Smith, M. D.; Long, G. J. *Inorg. Chem.* **2002**, *41*, 4453.

$Me_2pz)_3]_2\}(BF_4)_2$ from changing over to the low-spin state at low temperatures. Interestingly, the phase change causes the torsion angles of the second one-half of the metal dications to increase, favoring the low-spin form and explaining the highly cooperative spin-state crossover observed.[34b] Although we could not obtain a low-temperature X-ray structure of **3b** because the crystals shatter on cooling, it is likely that a phase change yields a similar change in the important FeN−NC torsion angles such that one-half of the high-spin iron(II) ions are prevented from changing over to the low-spin state at low temperatures.

The magnetic behavior of **4b** is highly unusual, and as a result, it provides insight into the nature of the spin-crossover behavior of poly(pyrazolyl)borate iron(II) complexes. First, the crystals are ordered in a three-dimensional network as a result of multiple CH−π interactions, but the crystals do not undergo any phase transition between 4 and 294 K. There is no hysteresis associated with the spin-state transition observed between 200 and 350 K, and there is little, if any, hysteresis associated with the spin-state crossover at 106 to 114 K. Two crystallographically independent iron(II) sites are found in the crystal, and the molecules containing Fe(1), the site with greater tilting of the pyrazolyl rings, undergo a spin-state crossover at the lower temperatures, whereas the Fe(2) containing molecules relax between the high-spin and the low-spin states at higher temperatures. Although the Fe(1) and Fe(2) sites are segregated into alternating sheets throughout the crystal, the same number of CH−π interactions hold each of the sheets together, indicating that the supramolecular structure is *not* responsible for the difference in behavior of the two iron sites. We propose that the greater degree of ligand pyrazolyl ring tilting at the Fe(1) site in the high-spin form, rather than the supramolecular structure, drives the difference in the temperature at which the electronic spin-state changes occur for the two independent iron(II) crystallographic sites. In other words, as the temperature is lowered, the Fe(2) site, with less pyrazolyl ring tilting, can relax to the low-spin state at a higher temperature because the structures are already more like that observed in the low-spin tris(pyrazolyl)borate complexes. In contrast, it takes a lower temperature for the Fe(1) site, with the larger pyrazolyl ring tilting, to switch to the low-spin state. These results parallel those observed for $\{Fe[HC(3,5\text{-}Me_2pz)_3]_2\}(BF_4)_2$ (see above) in which the phase change caused such a large increase of the pyrazolyl ring tilting that the spin-crossover was prevented at low temperature.

The abrupt nature of the low-temperature transition is likely to be due to the cooperative nature of the geometric changes that propagate throughout the noncovalent network of the crystals. The average distances for the CH−π interactions increase with increasing temperature as expected from 2.959 to 3.231 to 3.309 Å at 90, 150, and 294 K, respectively. If one assumes that these CH−π interactions are comparable with the dipole−dipole, dipole−induced dipole, or, perhaps more accurately, the dipole−quadrupole interactions, their energy decreases dramatically with distance as $1/r^3$ for the former interaction but as $1/r^6$ for the latter two interactions. Thus, it is not surprising that the higher temperature crossover is more gradual than the lower temperature crossover as the geometric changes that occur at the higher temperature are not as effectively propagated throughout the crystal because of the weaker noncovalent interactions.

Conclusions

The utility of using alkyne coupling reactions with the $Fe[(p\text{-}IC_6H_4)B(3\text{-}Rpz)_3]_2$ complex to derivatize trispyrazolylborate iron(II) complexes has been demonstrated. This reaction provides a wide range of new opportunities for the use of these third generation tris(pyrazolyl)borate ligands with many metal ions in a variety of applications. We show herein that changing substituents at the 4-position of the phenyl ring in the $Fe[(p\text{-}XC_6H_4)B(3\text{-}Mepz)_3]_2$ complexes has a profound effect on the magnetic behavior of these complexes, even though the substitution is distal from the FeN_6 central core. For X = Ph, Me_3Si, and H, we observe three very different types of spin-state behavior, changing from gradual with hysteresis, to an abrupt 50% crossover, to an unusual combination of a spin-state relaxation and a spin-state crossover, respectively. The behavior of the first two complexes is largely determined by phase transitions. We have been able to show that, with X = H, **4b**, the degree of pyrazolyl ring tilting in the high-spin structure, rather than the strength of the intermolecular forces that organize the supramolecular structure, plays the dominant role in determining the temperature of the spin-state crossovers. In a separate paper, which reported on the properties of the polymorphs of $Fe[(p\text{-}IC_6H_4)B(3\text{-}Mepz)_3]_2$, we showed spin-state crossover of the polymorphs was dominated by differences in the supramolecular structures.[6] Thus when comparing even very similar or identical complexes, both the supramolecular structure and the degree of pyrazolyl ring tilting of the ligands, which may be affected by the supramolecular structure, can control the temperature and characteristics of the spin crossover. For complexes undergoing phase changes, this presumably noncontrollable variable dominates the spin crossover.

Acknowledgment. We thank the National Science Foundation (CHE-0414239) and the Petroleum Research Fund (36368-AC3) for support. The Bruker CCD Single Crystal Diffractometer was purchased using funds provided by the NSF Instrumentation for Materials Research Program through Grant DMR:9975623. L.R. and F.G. acknowledge with thanks the financial support of the Fonds National de la Recherche Scientifique, Belgium, through Grant 9.456595, the Fonds de la Recherche Fondamentale Collective, Belgium, through Grant 2.4522.01, and the Ministère de la Région Wallonne for Grant RW/115012.

Supporting Information Available: CIF files for $Fe[(p\text{-}PhC_2C_6H_4)B(3\text{-}Mepz)_3]_2$, **2**, $Fe[(p\text{-}Me_3SiC_2C_6H_4)B(3\text{-}Mepz)_3]_2$, **3b**, and $Fe[(p\text{-}HC_2C_6H_4)B(3\text{-}Mepz)_3]_2$, **4b** (at three temperatures). Table 2S, the complete Mössbauer spectral hyperfine parameters for $Fe[(p\text{-}HC_2C_6H_4)B(3\text{-}Mepz)_3]_2$, **4b**. This material is available free of charge via the Internet at http://pubs.acs.org.

JA044900H